



Three-Dimensional Property Modelling of the Montney Formation in Alberta

AER/AGS Open File Report 2018-10

Three-Dimensional Property Modelling of the Montney Formation in Alberta

S. Lyster, F.H. Marshall, T.L. Playter and H. Berhane

Alberta Energy Regulator
Alberta Geological Survey

March 2019

©Her Majesty the Queen in Right of Alberta, 2019
ISBN 978-1-4601-3979-0

The Alberta Energy Regulator/Alberta Geological Survey (AER/AGS), its employees and contractors make no warranty, guarantee or representation, express or implied, or assume any legal liability regarding the correctness, accuracy, completeness or reliability of this publication. Any references to proprietary software and/or any use of proprietary data formats do not constitute endorsement by AER/AGS of any manufacturer's product.

If you use information from this publication in other publications or presentations, please acknowledge the AER/AGS. We recommend the following reference format:

Lyster, S., Marshall, F.H., Playter, T.L. and Berhane, H. (2019): Three-dimensional property modelling of the Montney Formation in Alberta; Alberta Energy Regulator / Alberta Geological Survey, AER/AGS Open File Report 2018-10, 45 p.

Publications in this series have undergone only limited review and are released essentially as submitted by the author.

Published March 2019 by:

Alberta Energy Regulator
Alberta Geological Survey
4th Floor, Twin Atria Building
4999 – 98th Avenue
Edmonton, AB T6B 2X3
Canada

Tel: 780.638.4491
Fax: 780.422.1459
E-mail: AGS-Info@aer.ca
Website: www.ags.aer.ca

Contents

1	Introduction.....	1
1.1	Objectives	1
2	Stratigraphic Framework.....	1
3	Model Definitions	3
4	Modelling Workflow	6
5	Model Inputs	7
5.1	Input Source Data	7
5.1.1	Stratigraphic Pick Data	7
5.1.2	Input Extent Data	10
5.1.3	3D Property Data	11
5.1.4	2D Property Data	14
5.2	Input Surface Interpolation	18
5.3	Input Surface Manipulation	19
5.4	Input Surface Uncertainty	21
6	Model Construction	23
6.1	Structural Framework	24
6.2	Facies Model	24
6.3	3D Property Model	24
6.3.1	Upscale Well-Log Data.....	26
6.3.2	Geostatistical Analysis.....	27
6.3.3	Populate 3D Geocellular Grid.....	31
6.4	2D Property Model	31
6.4.1	Upscaled Point Property Data.....	32
6.4.2	Geostatistical Analysis.....	33
6.4.3	Populate 2D Geocellular Grid.....	38
6.4.4	Upscaling to the 3D Grid	39
7	Model Outputs	39
7.1	Digital Data.....	40
7.2	iMOD 3D Visualization.....	41
8	Model Quality	41
9	Summary	43
10	References.....	44

Tables

Table 1: A summary of the interpolation details for the modelled surfaces.	21
Table 2: Univariate distribution values for the upscaled well-log variables.	28
Table 3: Variogram parameters for the gamma-ray variable in the 3D property model.	30
Table 4: Variogram parameters for the porosity variable in the 3D property model.	30
Table 5: Variogram parameters for the TOC variable in the 3D property model.	31
Table 6: Univariate distribution values for the upscaled point property variables.	36
Table 7: Variogram parameters for the variables in the 2D property model.	37
Table 8: Confidence level of all modelled horizons.	42
Table 9: Confidence level of all modelled properties.	43

Figures

Figure 1: Map showing the approximate extent of the Montney property model within Alberta.	2
Figure 2: An isometric view of the Montney property model.	3
Figure 3: Conceptual model of the Montney stratigraphic framework.	4
Figure 4: Map of the locations of 6698 picks used to model the top of the Montney Formation.	8
Figure 5: Map of the locations of 4006 picks used to model the sub-Triassic unconformity.	9
Figure 6: Map of the locations of 752 top and 758 base picks used to model the CDMM.	10
Figure 7: Map of the locations of 557 top and 556 base picks used to model the turbidite bodies.	11
Figure 8: Map of the extent polygons of the model, Montney Formation, CDMM, and turbidites.	12
Figure 9: Isometric view of the 6513 gamma-ray logs used for modelling.	13
Figure 10: Isometric view of the 534 porosity logs used for modelling.	13
Figure 11: Isometric view of the 534 TOC logs used for modelling.	14
Figure 12: Map of the 2032 pressure gradient data points used for modelling.	15
Figure 13: Map of the 2146 temperature gradient data points used for modelling.	16
Figure 14: Map of the 4804 gas-oil ratio data points used for modelling.	17
Figure 15: Map of the 11 260 condensate-gas ratio data points used for modelling.	18
Figure 16: Isometric view of the modelled Montney Formation top surface.	19
Figure 17: Isometric view of the modelled sub-Triassic unconformity.	20
Figure 18: Isometric view of the modelled CDMM and turbidite top surface.	20
Figure 19: Standard deviation map of the modelled Montney Formation top surface.	22
Figure 20: Standard deviation map of the modelled sub-Triassic unconformity modelled surface.	23
Figure 21: Isometric view of the facies model.	25
Figure 22: Isometric view of the 353 847 upscaled cells in the gamma-ray model.	26
Figure 23: Isometric view of the 63 986 upscaled cells in the porosity model.	27
Figure 24: Isometric view of the 71 795 upscaled cells in the TOC model.	27
Figure 25: Variogram model in siltstone for the gamma-ray variable in the 3D property model.	29
Figure 26: Isometric views of the gamma-ray model.	32
Figure 27: Isometric views of the porosity model.	33
Figure 28: Isometric views of the TOC model.	34
Figure 29: Isometric view of the 1752 upscaled cells in the pressure gradient model.	34

Figure 30: Isometric view of the 1850 upscaled cells in the temperature gradient model.....	35
Figure 31: Isometric view of the 3745 upscaled cells in the gas-oil ratio model.....	35
Figure 32: Isometric view of the 3219 upscaled cells in the condensate-gas ratio model.	36
Figure 33: Variogram model for the pressure gradient variable in the 2D property model.....	37
Figure 34: Isometric views of the pressure gradient model.	38
Figure 35: Isometric views of the temperature gradient model.	39
Figure 36: Isometric views of the gas-oil ratio model.	40
Figure 37: Isometric views of the condensate-gas ratio model.....	41

Acknowledgements

The authors would like to thank the AER and AGS staff who contributed their input and comments to this work, including Paulina Branscombe, Kelsey MacCormack, Mahshid Babakhani, Kirk McKay, and Matt Grobe.

Abstract

The Lower Triassic Montney Formation extends over a large area of west-central Alberta and is a major drilling target for unconventional oil and gas, with a significant amount of natural gas liquids. The Montney Formation is made up primarily of siltstone, and includes coquinas and turbidite deposits. A three-dimensional (3D) property model of the Montney Formation was created.

The model area covers approximately 88 000 km² and is bounded by the Alberta-British Columbia border in the west, the deformation edge associated with the Rocky Mountains to the southwest, and the erosional edge of the Montney Formation to the north and east. The volume of the model was defined by Montney Formation top and base surfaces that were interpolated from stratigraphic picks. Internal surfaces representing the top and base of the turbidite and coquina geobodies were interpolated.

Three properties were modelled in a 3D grid from petrophysical well-log analysis: gamma-ray response, total porosity, and total organic carbon. Four properties were modelled in two dimensions (2D) based on data that is more sparse and uncertain: pressure gradient, temperature gradient, gas-oil ratio, and condensate-gas ratio. The 2D properties were modelled to align with the 3D grid to allow for calculations using all of the properties. All of the properties were simulated using the Gaussian Random Function Simulation (GRFS) algorithm in Schlumberger Petrel 2015 (Petrel). In total, 100 realizations were simulated for each of the properties to represent the range of uncertainty in the model.

The model was created in Petrel and has been exported to non-proprietary formats for use in other software. A series of datasets from the 3D model is available for download in the form of deconstructed model products and digital data including;

- a deconstructed model dataset composed of discrete and continuous model horizons as Esri format grids, and zone model extent shapefiles,
- populated model properties as point data in ASCII format, and
- an iMOD model dataset package

All of the standard format digital datasets can be viewed in iMOD, an open source software, and Petrel, enabling users to visualize rotate, slice, explode, and toggle data on and off in 3D. The iMOD software provides users with an interactive geospatial environment where end users can manipulate 3D geological models and import their own geospatially referenced subsurface and surface data into it.

1 Introduction

The Alberta Geological Survey (AGS) 3D Provincial Geological Framework Model of Alberta, Version 1 (3D PGF model v1), was built to deliver geological information and convey geological understanding in an engaging three-dimensional (3D) geospatial environment (Branscombe et al., 2018a). The availability of modern methods and software makes it possible to fill in the skeleton of the 3D PGF model v1 with properties for individual volumes of rock. These properties can be used for quantitative purposes including resource calculations, identification of connectivity between subsurface units, delineation of geobodies in the subsurface, and quantification of geotechnical properties.

This report presents the methodology used to model the properties of the Montney Formation in west-central Alberta. [Figure 1](#) shows a map of the model boundary within Alberta. The model covers an area of about 88 000 km² and extends from Township 46 in the south to Township 103 in the north, and from Range 14, west of the 5th Meridian in the east to Range 14, west of the 6th Meridian in the west. For reference, [Figure 2](#) shows an isometric view of the Montney model within the 3D PGF model v1.

1.1 Objectives

This report documents the methodology used to develop a 3D geocellular model of properties in the Montney Formation. The report outlines the workflow and provides the parameters used during structural and property modelling. This allows critical evaluation of the modelling, aids reproducibility, and increases efficiency in future property modelling projects.

2 Stratigraphic Framework

The Montney Formation was deposited during the Early Triassic within the Western Canada Sedimentary Basin (Davies et al., 1997; Playter et al., 2018). It consists of sandstone, siltstone and coquina deposits and can reach a maximum thickness of 300 m (Edwards et al., 1994; Davies et al., 1997). Within Alberta, the Montney Formation is unconformably overlain by the Doig, Fernie, Cadomin, Gething and Bluesky formations (Edwards et al., 1994; Playter et al., 2018). The Montney Formation sits unconformably on Permian- and Carboniferous-aged deposits (Edwards et al., 1994; Playter et al., 2018). The Montney Formation is eroded by two major unconformities within Alberta: the sub-Jurassic unconformity and the sub-Cretaceous unconformity (Edwards et al., 1994; Playter et al., 2018). These unconformities mark the erosional limit of Montney Formation sedimentary strata, which thin eastward to the erosional edge.

Internal divisions within the Montney Formation are informally defined and, in Alberta, are based on the presence of the informally named Coquina Dolomite Middle member (CDMM), which marks the divide between the upper and lower Montney. However, this division is not possible where the CDMM does not exist. Instead, the presence of depositional clinofolds which can be correlated using biostratigraphy, chemostratigraphy and sedimentology, have been related to chronostratigraphic surfaces such as the Dienerian-Smithian and Smithian-Spathian boundaries (Playter et al., 2018). These chronostratigraphic surfaces can be used to subdivide the Montney in a consistent manner (Golding et al., 2014; Playter et al., 2018). The Dienerian-Smithian boundary marks a drop in sea level which correlates with the deposition

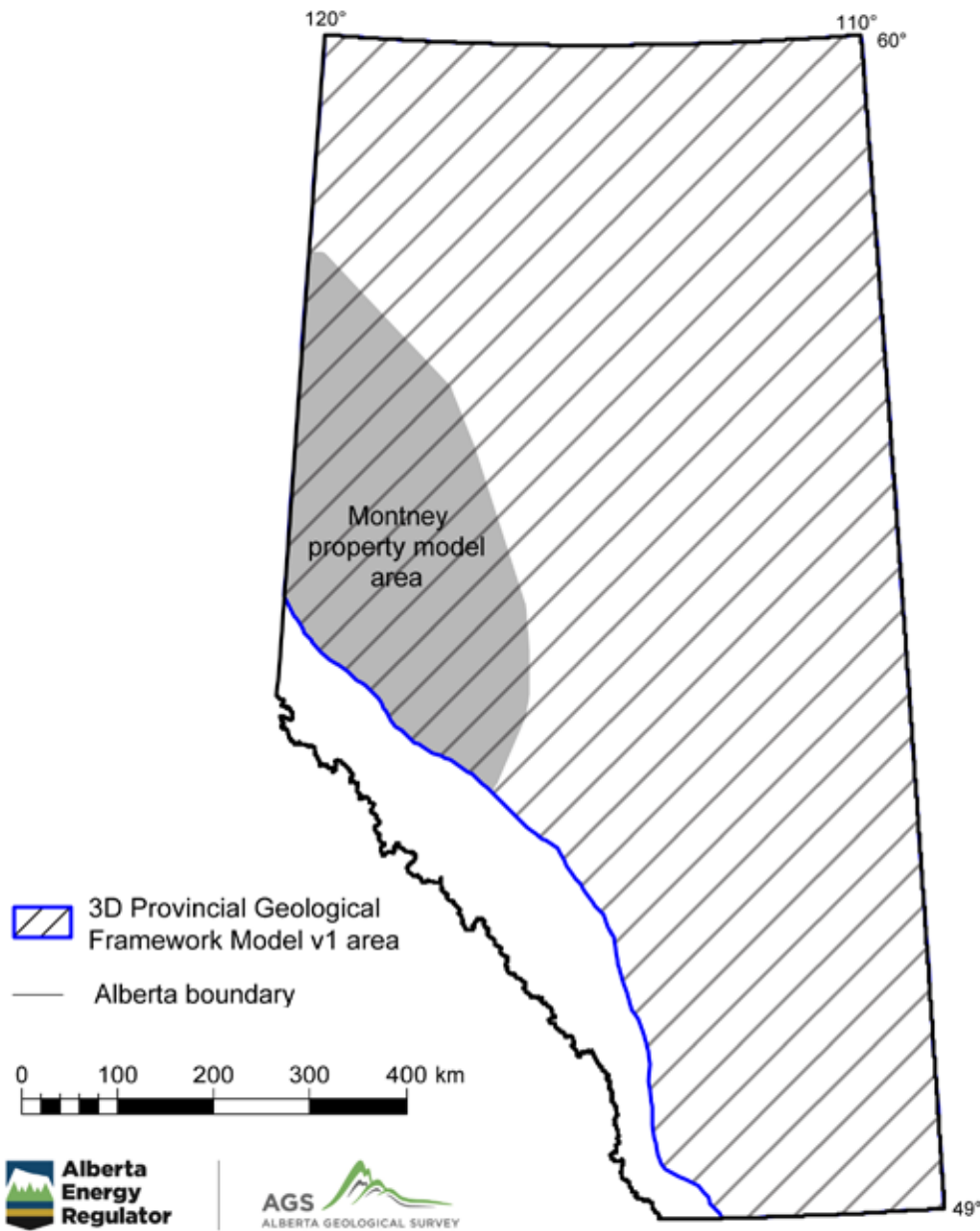


Figure 1: Map showing the approximate extent of the Montney property model (grey area) and that of the 3D PGF model v1 within Alberta.

of coquinas as well as turbidites within the Montney Formation (Davies et al., 1997). These deposits form some of the major reservoirs within the Montney Formation (Davies et al., 1997). Turbidite deposition within the Montney Formation was structurally controlled and largely confined within the structural lows of graben complexes along the Alberta-B.C. border, which formed following the collapse of the Peace River Arch (Davies et al., 1997). Recently, Zonneveld and Moslow (2018) proposed the subdivision of the Montney Formation into formal members, however, our work does not incorporate the newly proposed nomenclature.

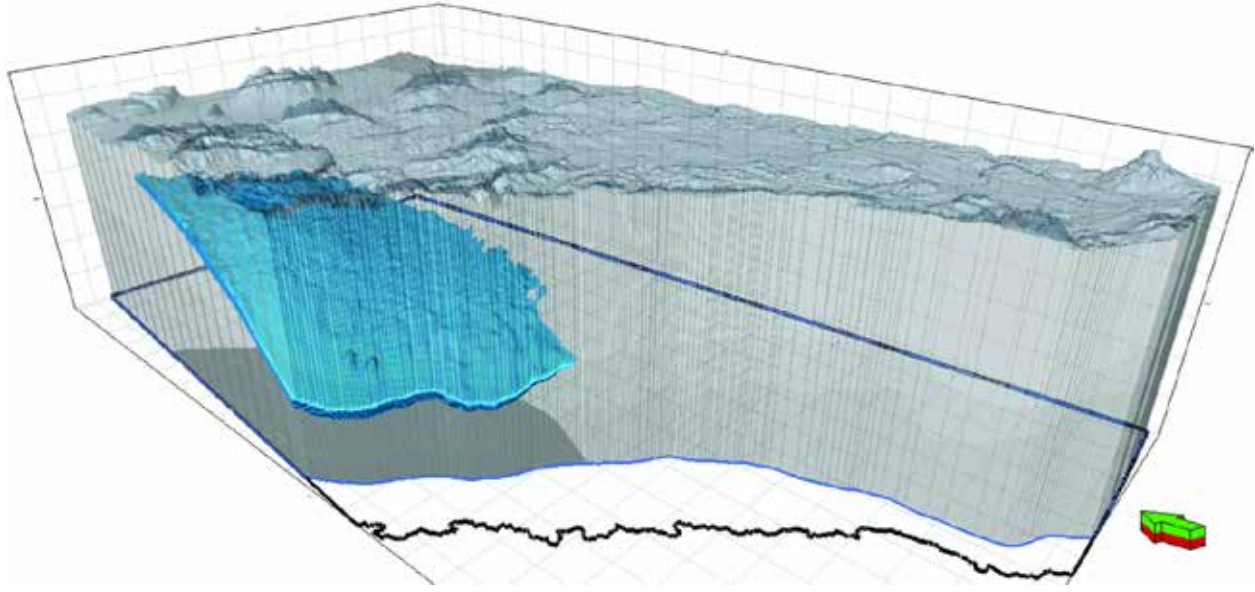


Figure 2: An isometric view of the Montney property model (solid blue) within the 3D PGF model v1 (transparent grey) (Branscombe et al., 2018b). Vertical exaggeration is 50 times.

For this project the stratigraphic framework of the Montney Formation was simplified to include only the top and base of the Montney Formation as well as those of the CDMM and turbidite bodies. The Dienerian-Smithian boundary is currently unmapped over most of the model area where the CDMM is not present. The Smithian-Spathian boundary is quite limited in extent in Alberta and the Smithian-aged uppermost part of the Montney was not separated out for modelling. [Figure 3](#) shows three diagrams of the conceptual model of the Montney used in this report, comparing to Davies et al. (1997), and Moslow and Davies (1997), as well as a generalized model column.

It is important to note that, in Alberta, there is a discrepancy between the definition of the geological top of the Montney Formation, as defined in the type well for the Montney and Doig formations (Armitage, 1962), and the regulatory definitions of the top of the Montney zone and the base of the Doig zone, as defined in the respective type wells for the deeper rights reversion zone designations 264 (Montney) and 251 (Doig) used for the administration of subsurface mineral rights by the Alberta Government (Alberta Energy, undated). In the work presented here, we use the geologically defined top of the Montney Formation. The geological top of the Montney Formation in Alberta is sometimes also referred to as the top of the lower Doig siltstone, a term introduced in unpublished consultant reports in the 1990s.

3 Model Definitions

The 3D property model of the Montney Formation has a variety of input and output data detailed in Section 5. The common terminology and definition of model inputs and outputs used in Branscombe et al. (2018a) have been expanded to include the terms ‘property’ and ‘property model’ and are provided below for reference.

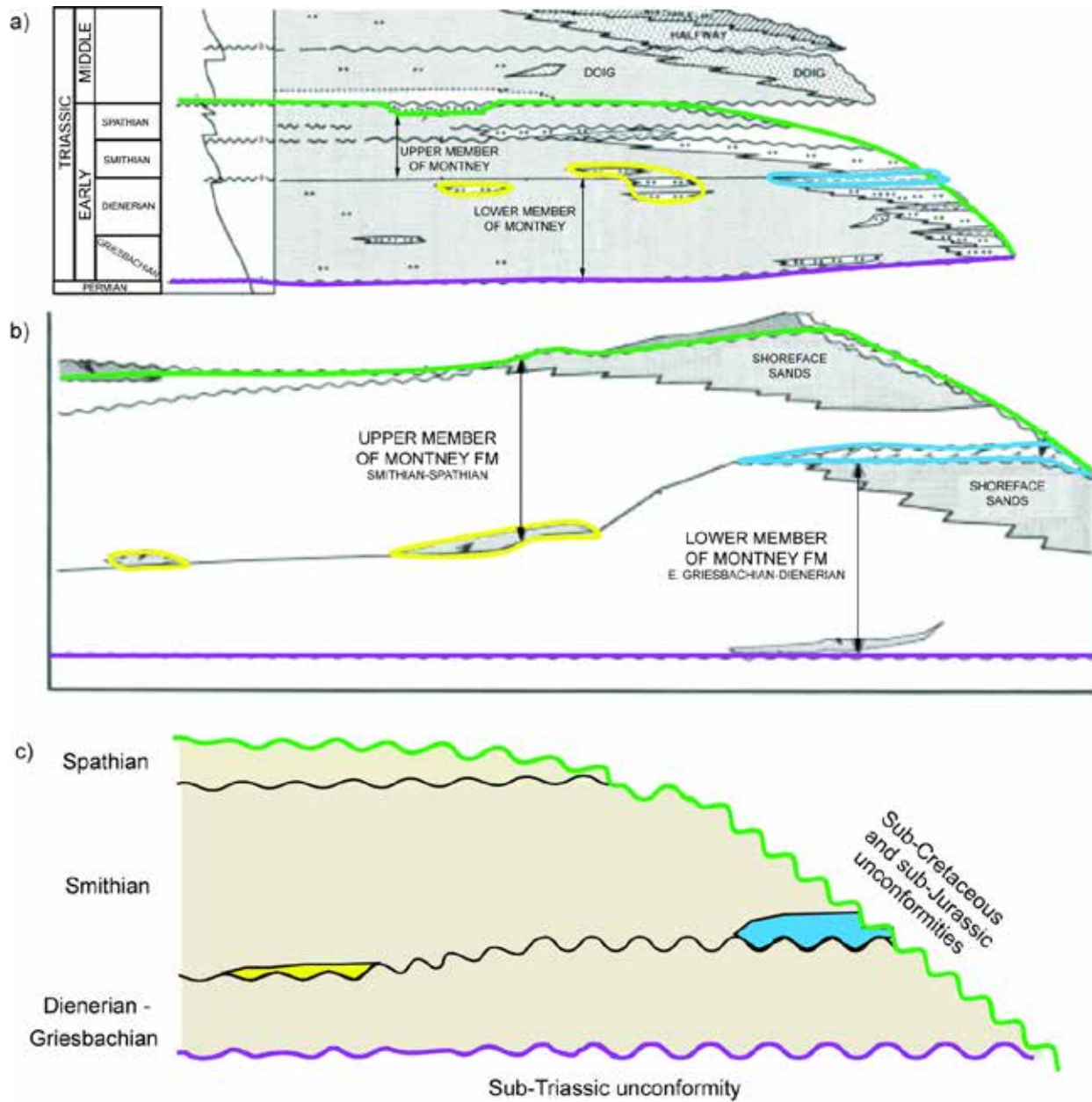


Figure 3: Conceptual model of the Montney stratigraphic framework for this report compared to previous work. a) After Davies et al. (1997); b) after Moslow and Davies (1997); c) generalized model column. Green: top of Montney Formation; purple: sub-Triassic unconformity; blue: Coquina Dolomite Middle member; yellow: turbidites.

Common Terminology

- **3D simple grid:** A simplified process/step when creating 3D grids with no faults in Petrel.
- **3D pillar grid:** A process/step when creating 3D grids that may or may not have faults in Petrel and more closely follows the model boundaries. More robust than the *3D simple grid* process.
- **3D geocellular grid:** A 3D geological model divided into cells/voxels resulting from the *3D simple grid* or *3D pillar grid* process.
- **discrete surface:** An interpolated surface that does not span the entire model extent (see *interpolated*

surface).

- **property:** A value that represents a physical or reservoir characteristic of a defined volume of rock.

Model Inputs

- **source data:** A set of unfiltered, original, multi-source point data defining the stratigraphic pick of a zone top or base. These data include geospatial coordinates (x, y) and elevation (z) information. Most of the data are from well boreholes and have a unique well identifier (UWI), however, a UWI is not provided for outcrop or lineament sampled data.
- **input filtered data:** A set of geostatistically filtered, multi-source point data defining the stratigraphic pick of a zone top or base. These data include UWI, geospatial coordinates (x, y), and elevation (z) information. This dataset excludes outliers and erroneous data captured in the *source data*. The outliers and erroneous data were eliminated in a series of successive culls to reduce global uncertainty.
- **input extent / lineament(s):** A set of discrete polygons or polylines delineating a zone top or base zero-edge, subcrop edge, or other GIS information outlining a zone top or base and attributed with elevation (z) values.
- **interpolated surface:** A discrete gridded surface interpolated in modelling software over the geospatial extent of a zone top or base from *input filtered data* and *input extents / lineaments* (if applicable). Defines the elevation (z) of a zone top or base and is manipulated where necessary to eliminate cross-overs with adjacent *interpolated surfaces* and/or to honour unconformities. *Interpolated surfaces* are considered primary input data for the construction of a model and are used to constrain the top and base of a model as well as discretizing the model within. Each *interpolated surface* is defined as a particular type to define the geological relationship to other contacts (e.g., erosional, conformable, etc.), which ensures the geospatial and temporal relationships of all zone tops and bases are honoured.
- **geo-edge:** A set of polygons or polylines used to constrain (or clip) an *interpolated surface* to areas where the zone is present, as defined by a zero-edge and/or a subcrop-edge. *Geo-edges* are primarily defined by the geologist or geomodeller based on the distribution of zone stratigraphic picks and/or from external supporting data such as previously published literature.
- **continuous surface:** A gridded surface generated from discrete *interpolated surfaces* and modelled to span the entire model extent. Although a formation may only exist in part of the province, the surface must be modelled to cover the entire province to ensure the zone is completely sealed for continuous style model construction. To do this, we merge the discrete surface with the nearest surface or unconformity if the discrete surface is subcropping or outcropping.

Model Construction Outputs

- **model tabular point data:** The set of finalized stratigraphic picks selected from the *input filtered data* with lowest global uncertainty; published with UWI, geospatial coordinates (x, y), elevation (z) and dataset source for zone top and bases as a point dataset.
- **model extent:** A polygon that defines the boundary of a zone top or base *model horizon* and is attributed with elevation (z) values.
- **model horizon:** A grid that represents the 3D distribution and elevation of a zone top or base. It

captures the geospatial extent and elevation (z) values of discrete *interpolated surfaces*; however, where sufficient minimum vertical 3D geocellular grid cell sizes are not achieved, the horizon does not exist. The collection of all model horizons partitions the 3D geocellular grid into a series of *model zones*.

- **model zone:** Defines the vertical resolution of the 3D simple grid between *model horizons*.
- **model:** The combination and construction of all model zones in correct stratigraphic sequence.
- **property model:** The populated geocellular grid with defined property values for all cells/voxels with nonzero volumes.

4 Modelling Workflow

This section outlines the AGS Property Modelling Workflow that is an extension of the current AGS Geomodelling Workflow (Branscombe et al., 2018a). The AGS Property Modelling Workflow focuses on populating a 3D geocellular grid with properties after the framework model construction is complete, and expands on Part 5, Model Construction.

The current AGS Geomodelling Workflow is grouped into six main steps described below:

Part 1: Input Data and Stratigraphic Framework (Section 5.1)

- a. compile all source data (input points, lineaments and extents)
- b. combine multisource input data defining the top and base of each zone
- c. establish conceptual geological model(s) and convey to geomodeller(s)
- d. done by geologists and geomodellers

Part 2: Geostatistical Analysis

- a. geostatistically filter source data
- b. achieve stabilization of global uncertainty
- c. completed by geomodellers

Part 3: Input Surface Interpolation and Manipulation (Sections 5.2 and 5.3)

- a. create interpolated surfaces for tops and bases of zones
- b. manipulate interpolated surfaces to honour unconformable surfaces
- c. manipulate interpolated surfaces to ensure no crossovers with adjacent surfaces
- d. manipulate interpolated surfaces to geo-edges (if applicable)
- e. assess alignment with conceptual model(s)
- f. completed by geomodellers

Part 4: Uncertainty Analysis (Section 5.4)

- a. provide uncertainty analysis for interpolated surfaces
- b. completed by geomodellers

Part 5: Model Construction (Section 6)

- a. generate a 3D geological model of all zones from specified input parameters (Section 6.1)

- b. populate properties model
 - i. facies model (Section 6.2)
 - ii. 3D property model (Section 6.3)
 - iii. 2D property model (Section 6.4)
- c. completed by geomodellers

Part 6: Model Dissemination (Section 7)

- a. disseminate deconstructed 3D model outputs
- b. disseminate iMOD package for 3D visualization of model
- c. completed by geomodellers

The AGS Geomodelling Workflow has three main phases, the pre-construction phase (Parts 1 to 4), the construction phase (Part 5), and the dissemination phase. This report focusses on model construction in Part 5.

5 Model Inputs

This section describes the pre-construction front-end phase of the workflow. Detailed information about the model input data, surface interpolation, surface manipulation, and uncertainty analyses are provided in Sections 5.1 through 5.4.

5.1 Input Source Data

The input source data for the Montney Formation property model includes four data sets: stratigraphic pick data, extent data for the units, 3D property data (from well logs), and 2D property data (from production well tests). The 3D PGF model v1 does not include the Montney Formation, so the surfaces that were used to build the structural framework of the model were generated using stratigraphic pick data and zero-edge extents. The properties themselves were derived from well-log data that are continuous over a sample interval and property data in discrete points that are only sampled at specified x,y locations and do not have vertical resolution.

5.1.1 Stratigraphic Pick Data

The top of the model is defined by the top of the Montney Formation, as defined geologically (Armitage, 1962; Davies et al., 1997, 2018; Zonneveld and Moslow, 2018). The Montney Formation is eroded by several different unconformities to the east, and is uneroded in the west. For this model the top of the Montney was modelled as a single surface. There were 6698 stratigraphic picks of the eroded and uneroded top of the Montney Formation ([Figure 4](#)). These are all high-quality picks made by AGS geologists.

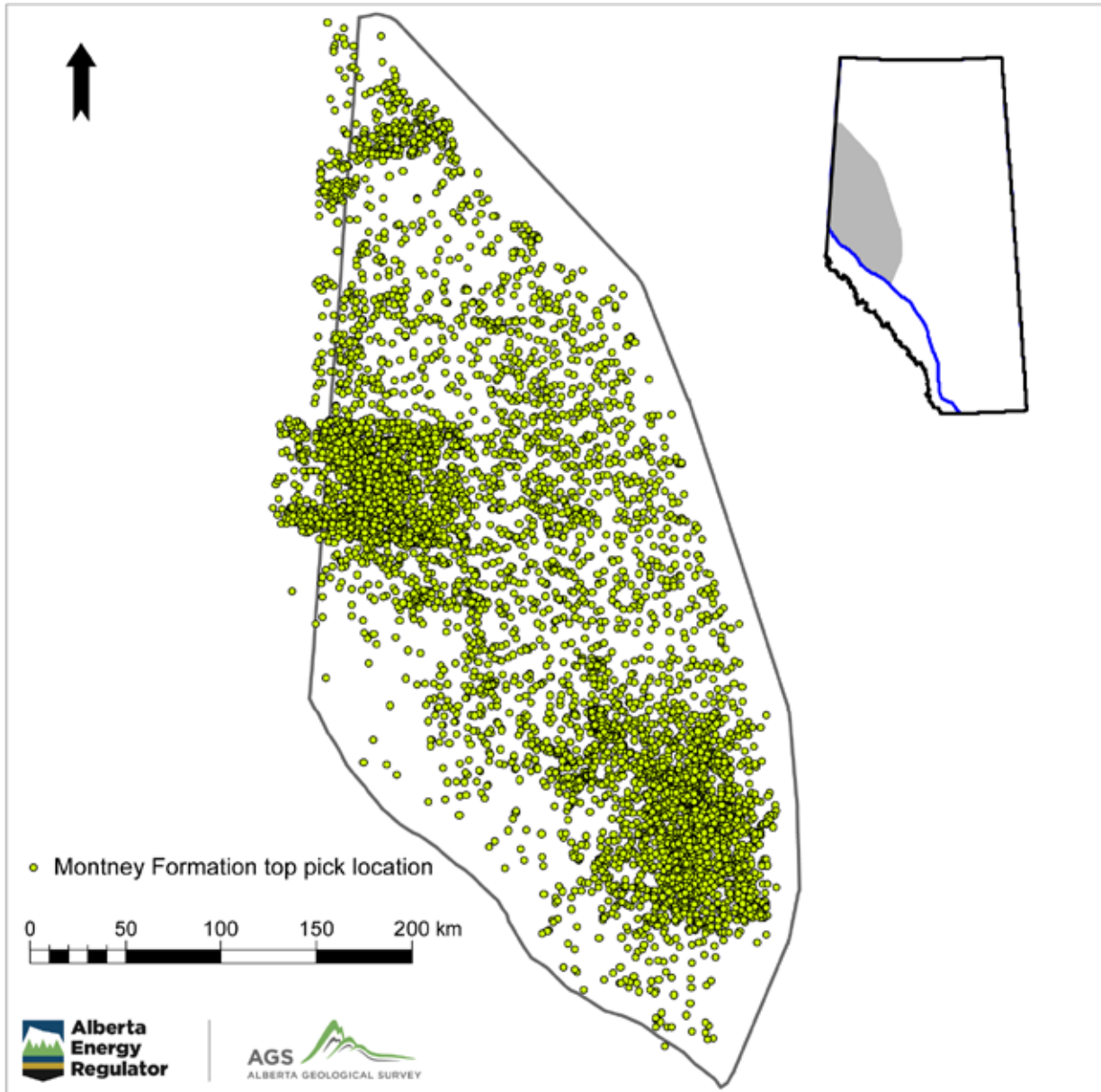


Figure 4: Map of the locations of 6698 picks used to model the top of the Montney Formation.

The base of the model is the base of the Montney Formation, which coincides with the sub-Triassic unconformity. There were 4006 picks of the sub-Triassic unconformity ([Figure 5](#)). These are all high-quality picks made by AGS geologists.

Within the Montney Formation, the CDMM was identified as a significant unit to separate out, because it marks the boundary between the lower and upper Montney at the Dienerian-Smithian boundary. To the east where much of the upper Montney is eroded, the CDMM represents the top of the eroded Montney Formation (see [Figure 3](#)). There were 752 picks for the top of the CDMM and 758 picks for the base ([Figure 6](#)). These are all high-quality picks made by AGS geologists.

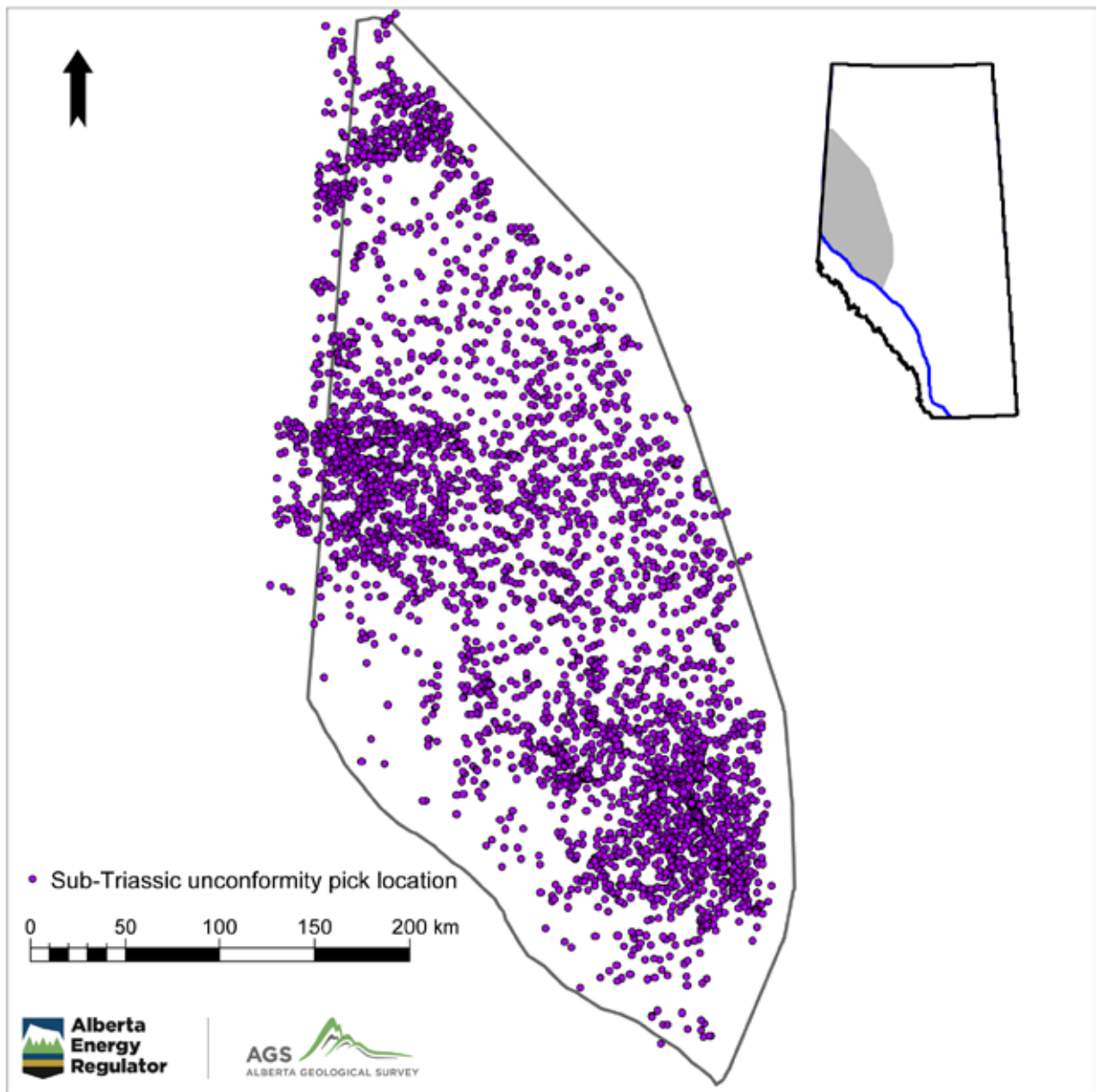


Figure 5: Map of the locations of 4006 picks used to model the sub-Triassic unconformity (base of Montney Formation).

A series of turbidite bodies within the Montney Formation was separated out as a separate unit for modelling. Several of these turbidites are interpreted to have been deposited near the Dienerian-Smithian boundary (see [Figure 3](#)). There were 557 picks for the tops of the turbidites and 556 picks for their base ([Figure 7](#)). These are all high-quality picks made by AGS geologists.

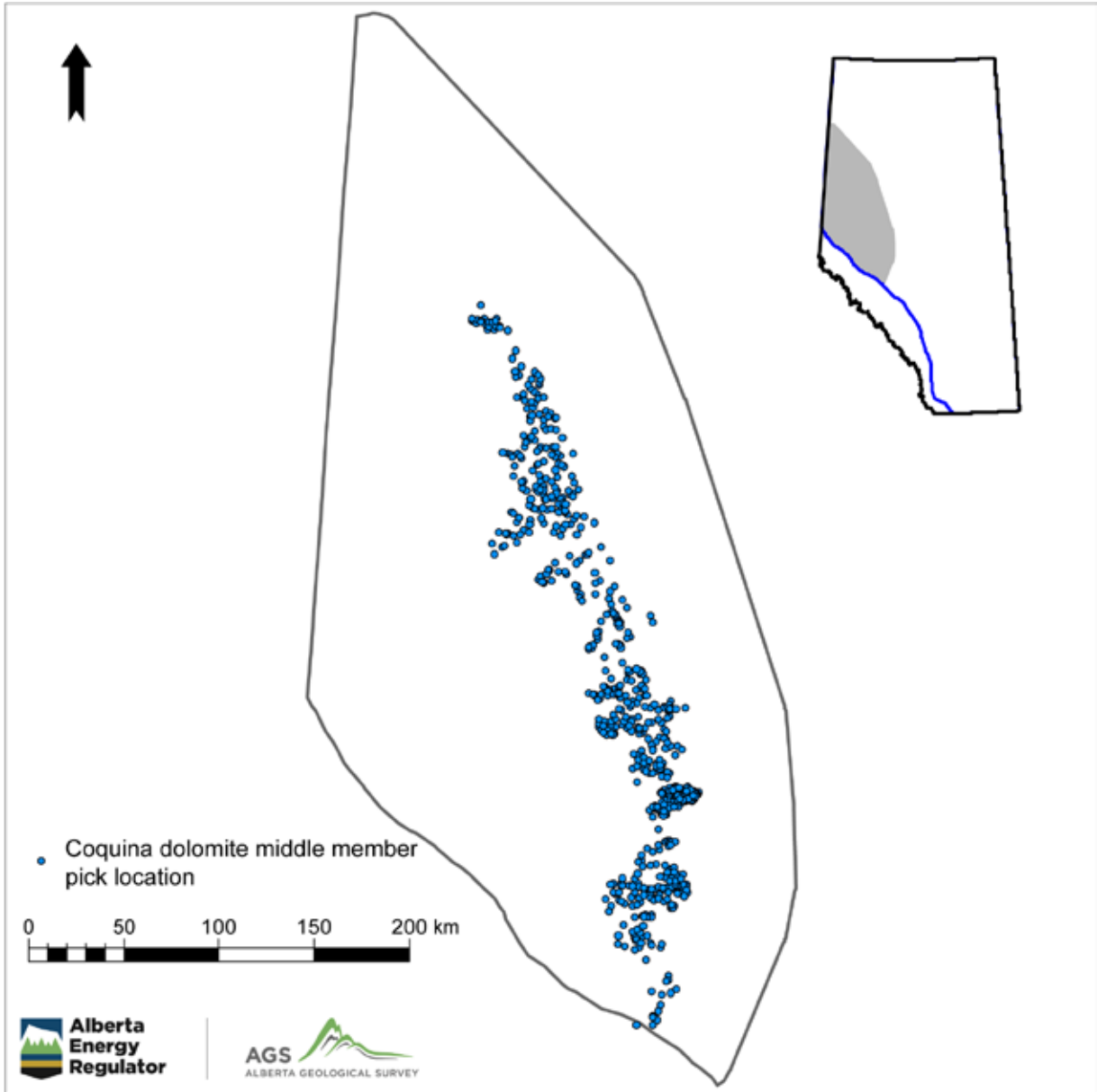


Figure 6: Map of the locations of 752 top and 758 base picks used to model the CDMM.

5.1.2 Input Extent Data

The model outline was set with a western boundary at the Alberta–British Columbia border; a southwestern boundary at the approximate deformation edge of the Rocky Mountains; and an eastern boundary that is a convex hull of the Montney Formation erosional edge, expanded by 10 km. The erosional edge of the Montney Formation was used to constrain the locations of cells in the model with non-zero volumes. Depositional/erosional extents for the CDMM and turbidite bodies were also provided by AGS geologists. These extents are not taken to be final or complete as there could still be adjustments or new bodies identified in the future. [Figure 8](#) shows a map of the extent polygons used to build the model.

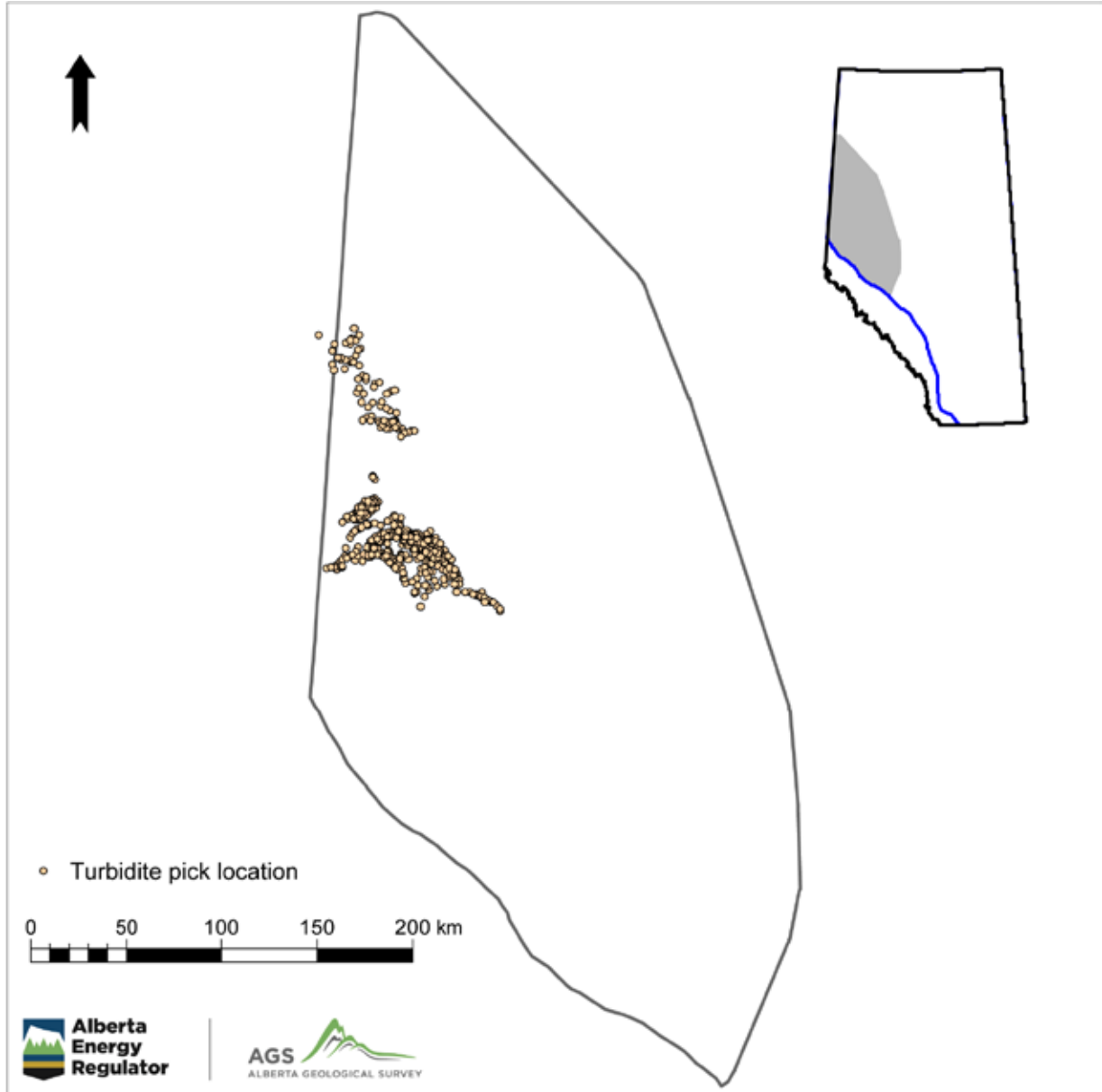


Figure 7: Map of the locations of 557 top and 556 base picks used to model the turbidite bodies.

5.1.3 3D Property Data

Well logs were used as the primary input for the Montney Formation properties modelled in 3D. Three properties were calculated from logs: gamma-ray response; total porosity; and total organic carbon (TOC).

The gamma-ray logs were assessed for quality by an AGS petrophysicist (534 logs) and extracted from the AGS LAS file holdings with lesser quality control (5979 logs). The logs with obvious outliers (negative values or values several times too high) were removed. The remaining data values were

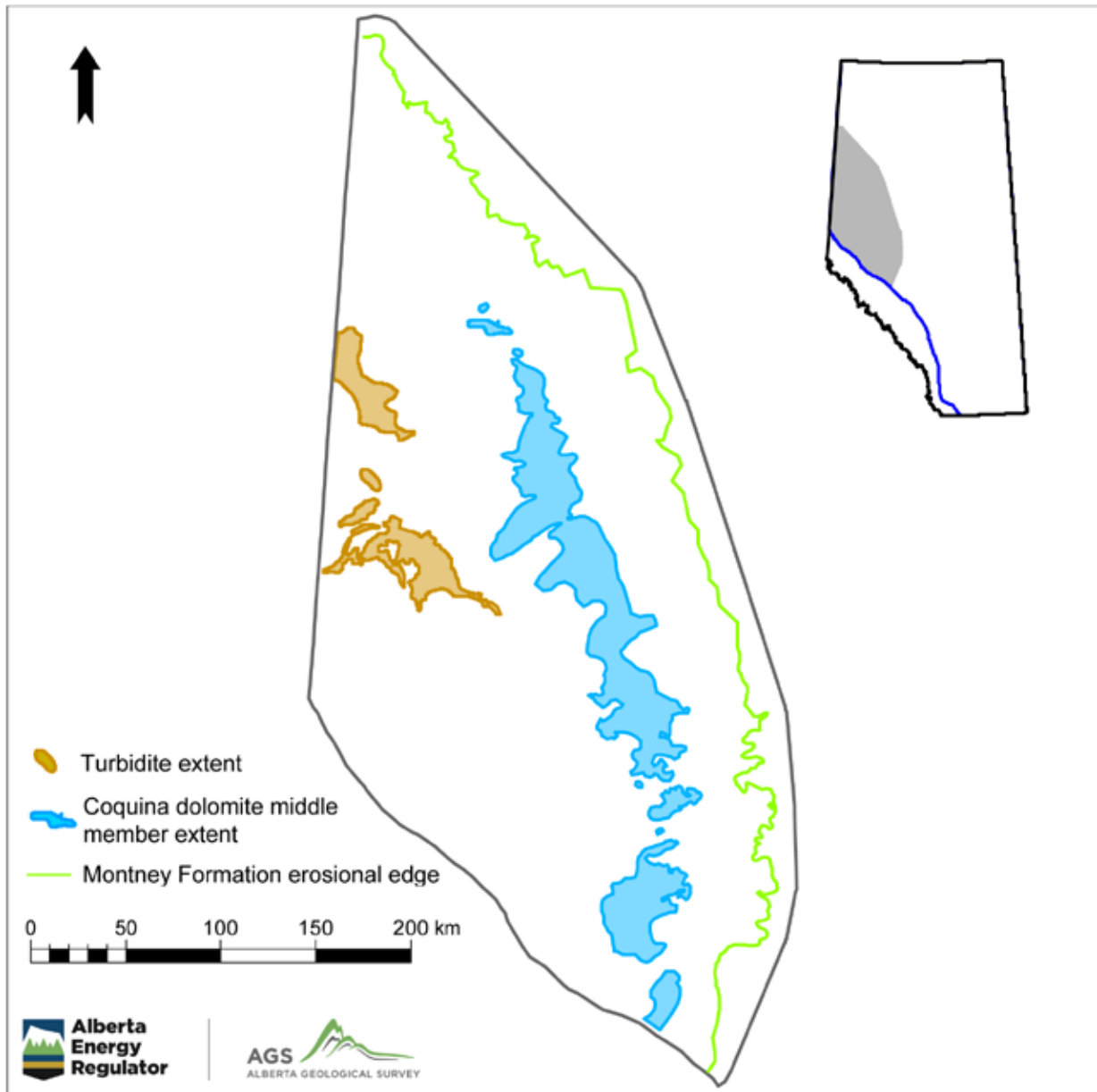


Figure 8: Map of the extent polygons of the model (grey), Montney Formation (green), CDMM (blue), and turbidites (brown).

truncated to a range of 25 to 175 API. [Figure 9](#) shows an isometric view of the 6513 gamma-ray logs used as inputs to the property model.

The porosity logs were interpreted by an AGS petrophysicist. The porosity was calculated from density logs accounting for the amount of TOC in the formation (TOC reduces the matrix density and affects the calculations). Values were truncated to 0.0001 (or 0.01%) at the low end to correct for log readings where local matrix density variations led to negative calculated porosity. [Figure 10](#) shows an isometric view of the 534 porosity logs used as inputs to the property model.

The TOC logs were interpreted by an AGS petrophysicist using Passey's method (Passey et al., 1990).

Figure 11 shows an isometric view of the 534 TOC well logs used as inputs to the property model.

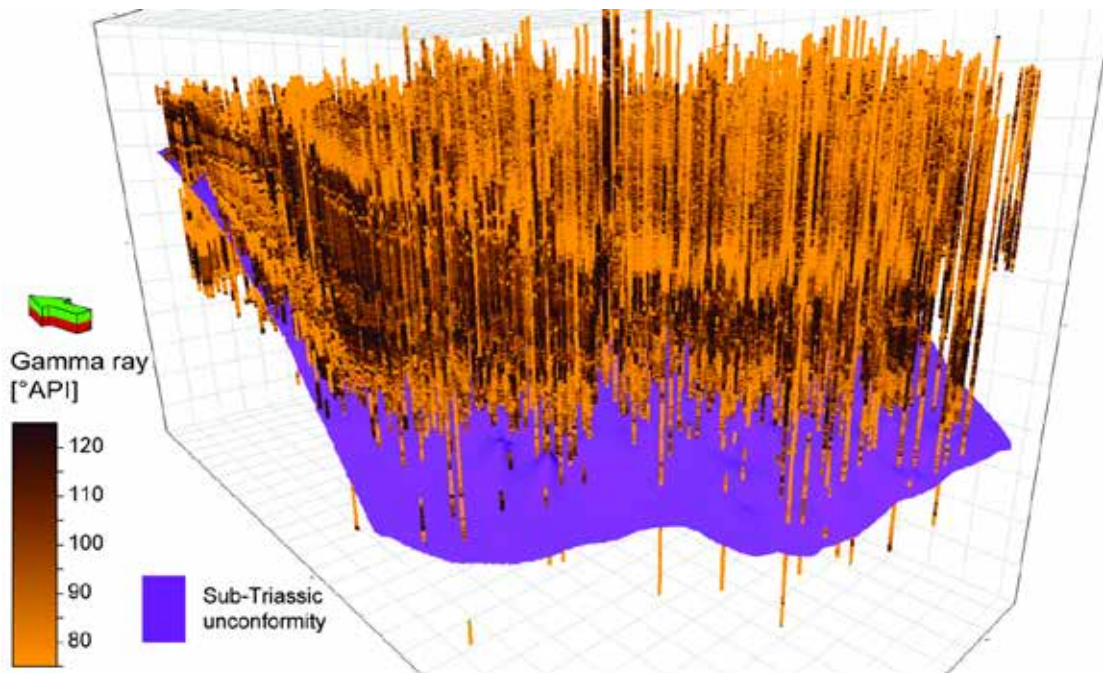


Figure 9: Isometric view of the 6513 gamma-ray logs used for modelling. The sub-Triassic unconformity surface (purple) is shown for spatial reference. Vertical exaggeration is 50 times.

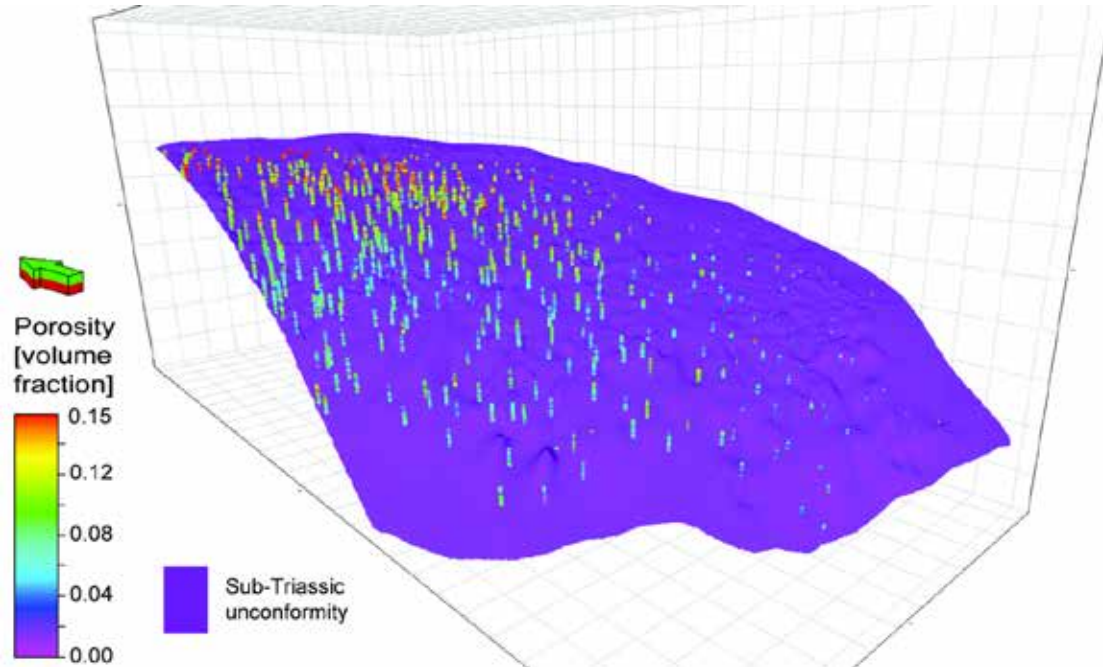


Figure 10: Isometric view of the 534 porosity logs used for modelling. The sub-Triassic unconformity surface (purple) is shown for spatial reference. Vertical exaggeration is 50 times.

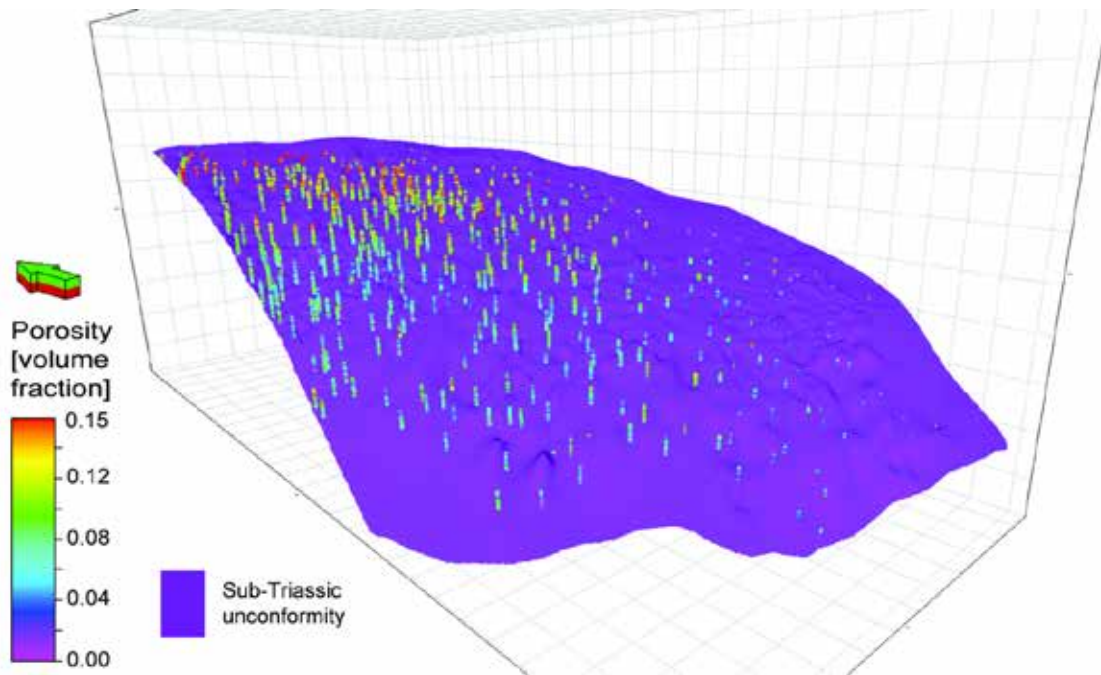


Figure 11: Isometric view of the 534 TOC logs used for modelling. The sub-Triassic unconformity surface (purple) is shown for spatial reference. Vertical exaggeration is 50 times.

5.1.4 2D Property Data

Calculating hydrocarbon resources requires quantification of many properties of the reservoir. The rock properties can be calculated from well logs as above. Other information about the state of the reservoir is taken from well tests, production history, and produced-gas analyses. These data types do not have the resolution necessary to differentiate between the top and bottom of a formation, and so are represented by points at the specified x and y locations but with z information assigned to the middle of the geological unit to conform to the model. Four properties were modelled using discrete point data: pressure gradient; temperature gradient; gas-oil ratio; and condensate-gas ratio.

Pressure gradient and temperature gradient values were taken from test data for wells reported as producing from the Montney. Those tests with missing data values, results out by orders of magnitude, or that disagreed with nearby data by a significant amount were removed. [Figure 12](#) shows a map of the 2032 pressure gradient point data used for modelling. [Figure 13](#) shows a map of the 2146 temperature gradient point data used for modelling.

Gas-oil ratio values were calculated from the production history of wells with at least 2160 producing hours (90 continuous days) reported as producing from the Montney. [Figure 14](#) shows a map of the 4804 gas-oil ratio point data used for modelling.

Condensate-gas ratio data were calculated from gas test data from wells that were reported as producing from the Montney. A relationship between different hydrocarbon proportions and the expected liquids production was used to convert the gas test data to a single value that could be modelled (Lyster, 2013).

Figure 15 shows a map of the 11 260 condensate-gas ratio point data used for modelling. Many of the point data locations have multiple tests that were dealt with at the upscaling step (Section 6.4.1).

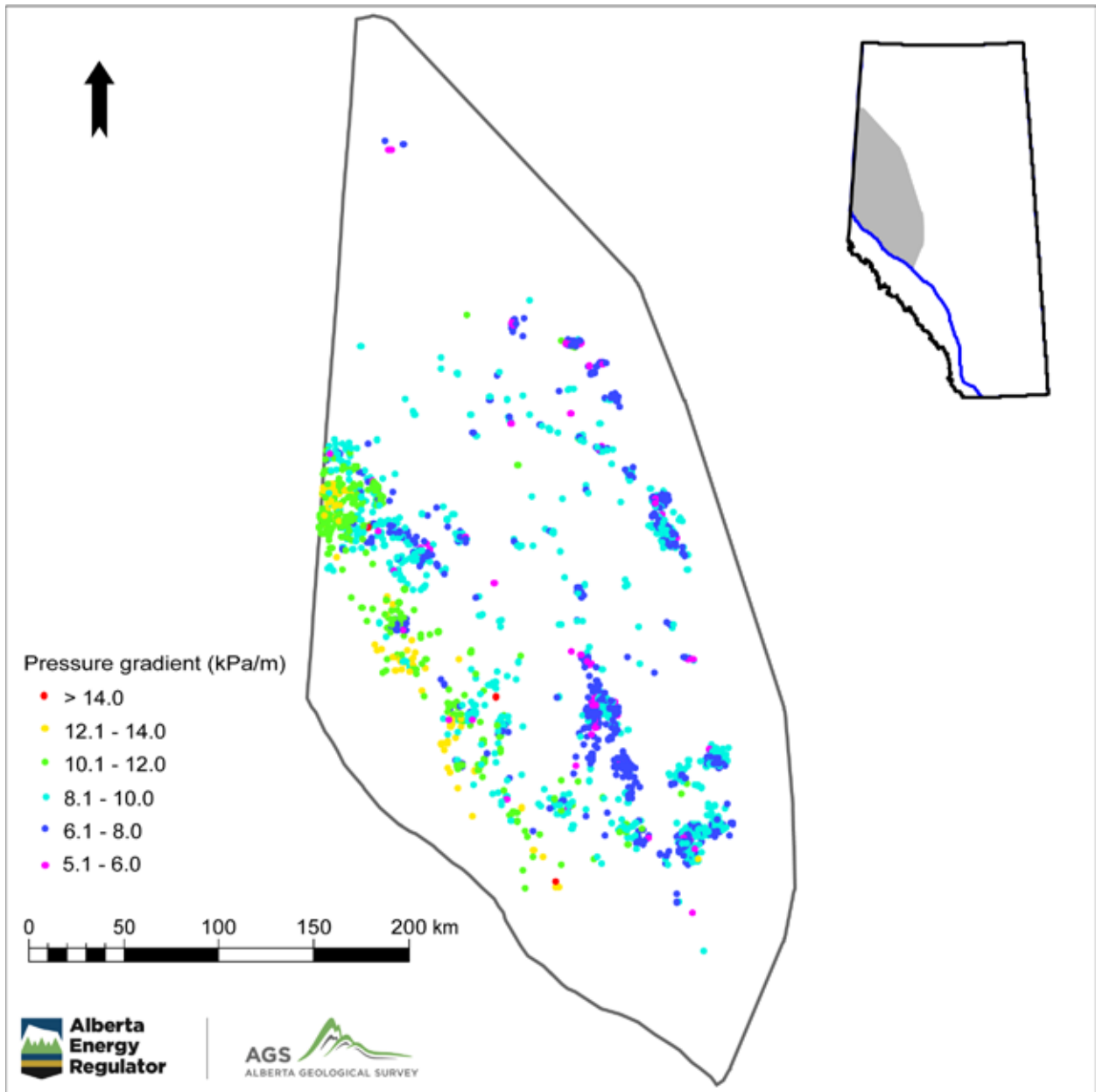


Figure 12: Map of the 2032 pressure gradient data points used for modelling.

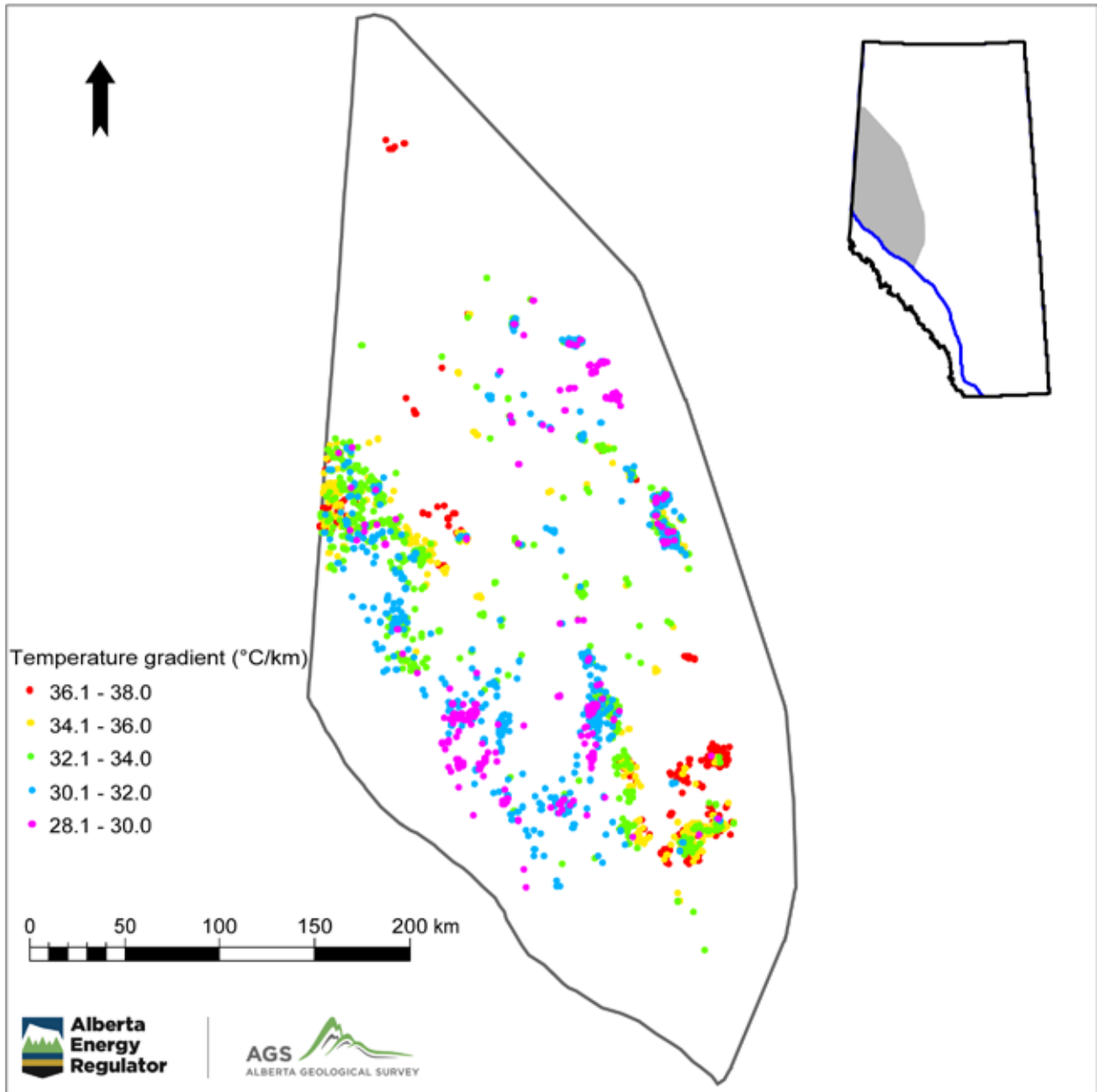


Figure 13: Map of the 2146 temperature gradient data points used for modelling.

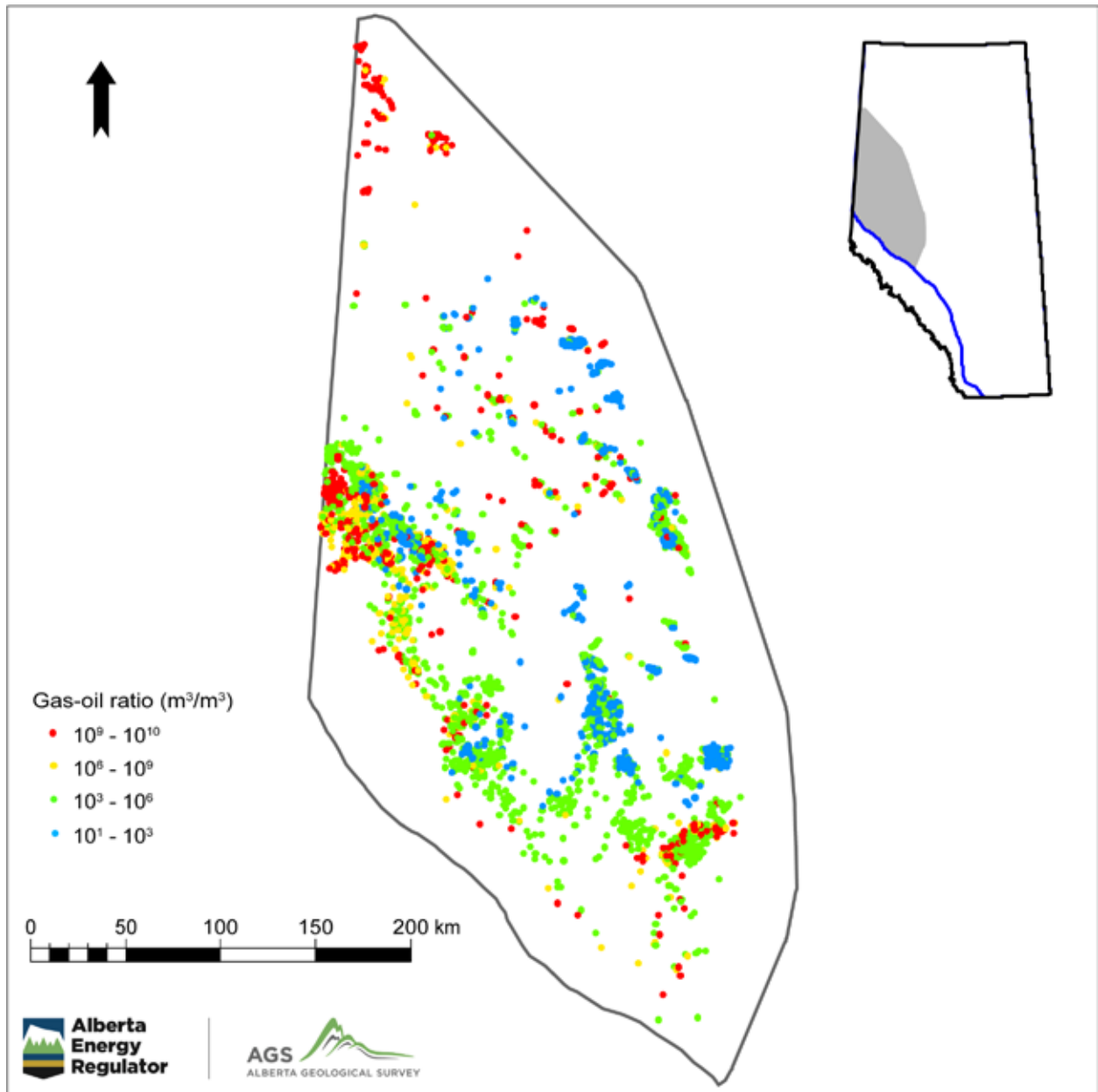


Figure 14: Map of the 4804 gas-oil ratio data points used for modelling.

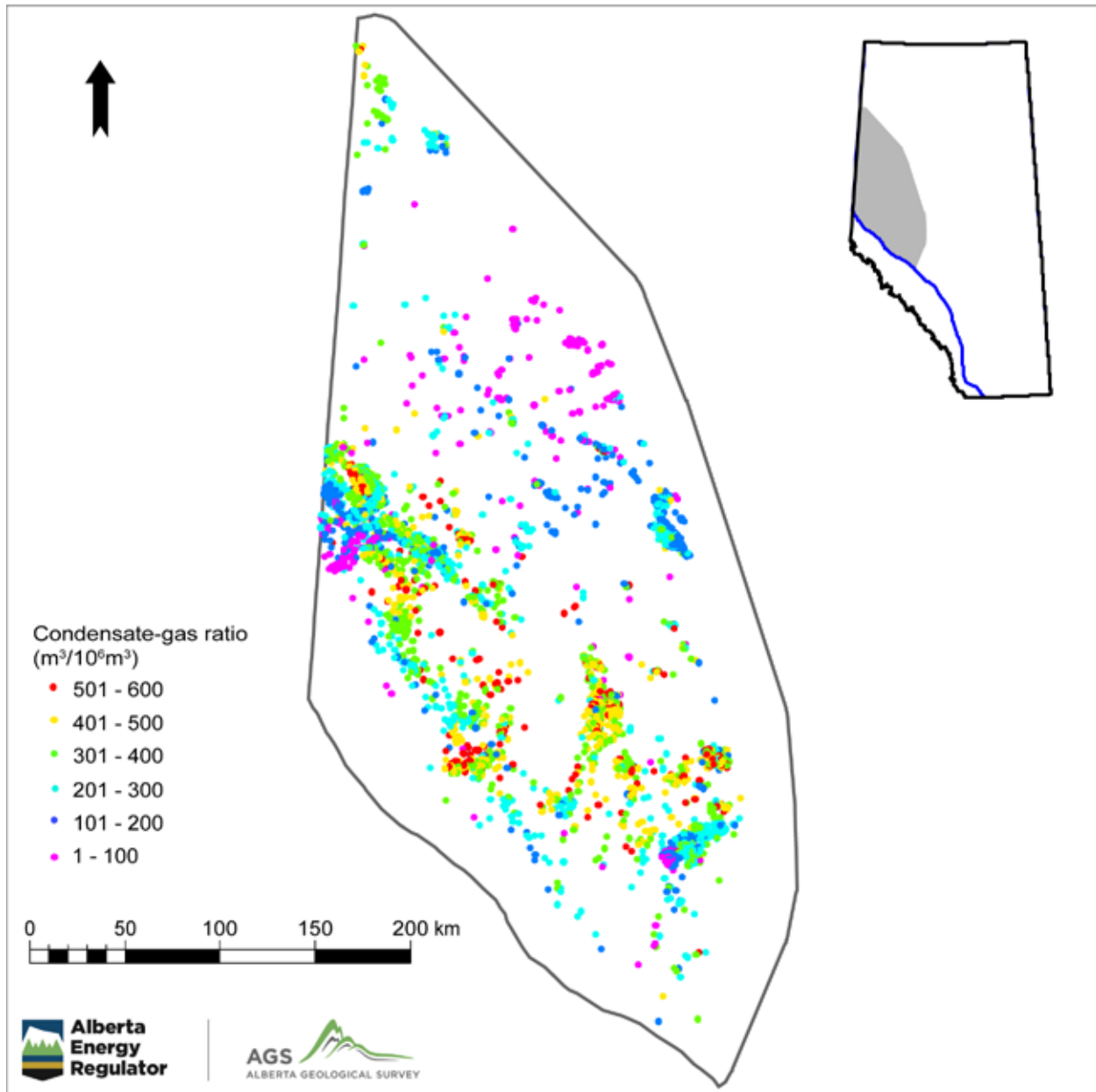


Figure 15: Map of the 11 260 condensate-gas ratio data points used for modelling.

5.2 Input Surface Interpolation

The surfaces that make up the structure of the Montney property model were created from stratigraphic pick data using the convergent interpolation and conformal gridding algorithms in Petrel 2015. The structural/stratigraphic surfaces (Montney Formation top and sub-Triassic unconformity) were interpolated as continuous surfaces over the entire model area. The top and base surfaces of the CDMM and turbidites were interpolated as discrete surfaces covering only the specific extents of the units. The interpolated surfaces were manipulated where necessary to ensure consistency in the geology of the 3D pillar grid (see Section 5.3). The surfaces were all visualized in 3D space to ensure consistency with one another and to identify any visually obvious potential outlier picks, which were sent back to the geologist

for re-examination.

Figure 16 shows an isometric view of the modelled top of the Montney Formation. The surface dips towards the southwest (towards the viewer); this is visible both in the surface and the colour scale. Figure 17 shows an isometric view of the modelled sub-Triassic unconformity (base of the Montney Formation). The top and base of the Montney are very similar in their elevation trends. Figure 18 shows an isometric view of the top of the CDMM and turbidites. The turbidites are lower within the Montney in the western part of the study area, and the CDMM subcrops at the eroded top of the Montney Formation towards the east.

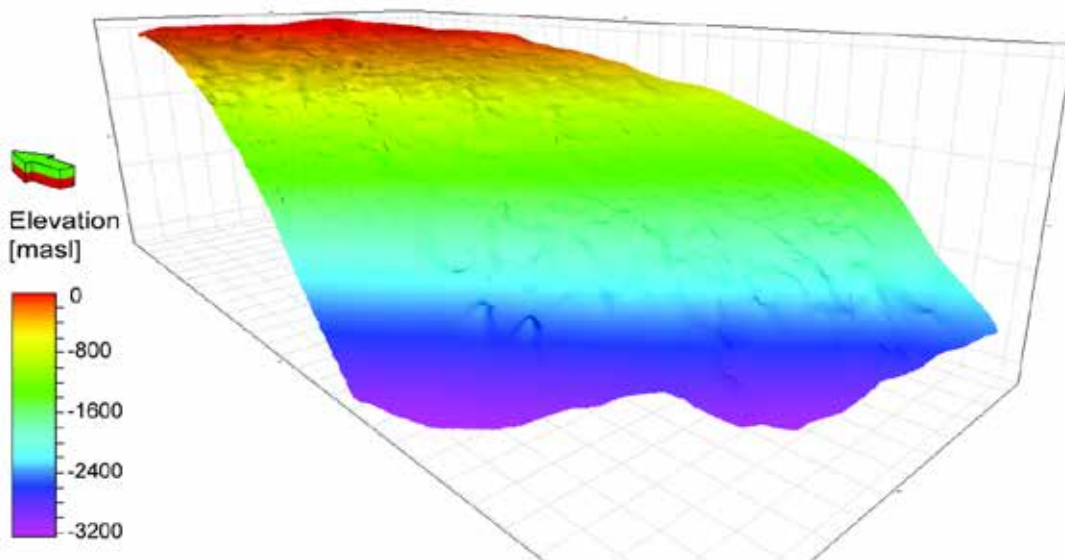


Figure 16: Isometric view of the modelled Montney Formation top surface. Vertical exaggeration is 50 times.

5.3 Input Surface Manipulation

The interpolated surfaces were manipulated where necessary to ensure that the structural framework does not have intersecting surfaces or negative thicknesses. This was done as part of the workflow during interpolation. Table 1 shows a summary of the steps in creating the model surfaces.

The sub-Triassic unconformity surface was interpolated first using the Convergent Interpolation algorithm in Petrel. The Montney Formation top surface was modelled to conform to the sub-Triassic unconformity and not be below the top CDMM picks. The base surface of the CDMM was modelled conformal to the sub-Triassic unconformity and corrected to not be above the Montney Formation top. The top surface of the CDMM was modelled conformal to the base of the CDMM and corrected so as not to be above the top of the Montney Formation, and be at the top of the Montney where it subcrops at the sub-Jurassic unconformity. The CDMM and turbidite surfaces were modelled to ensure that both of those units have non-negative thicknesses.

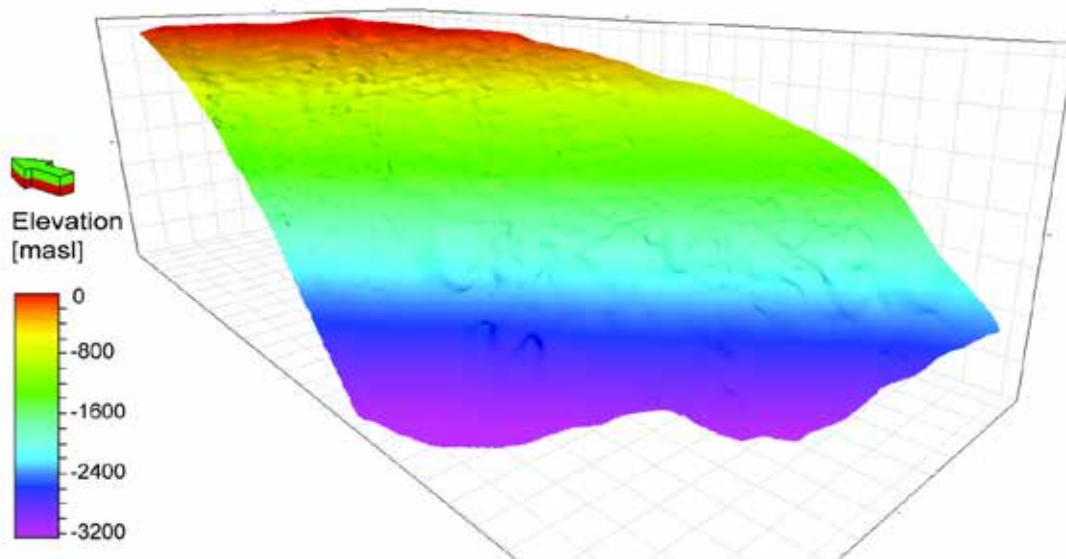


Figure 17: Isometric view of the modelled sub-Triassic unconformity (base of the Montney Formation) surface. Vertical exaggeration is 50 times.

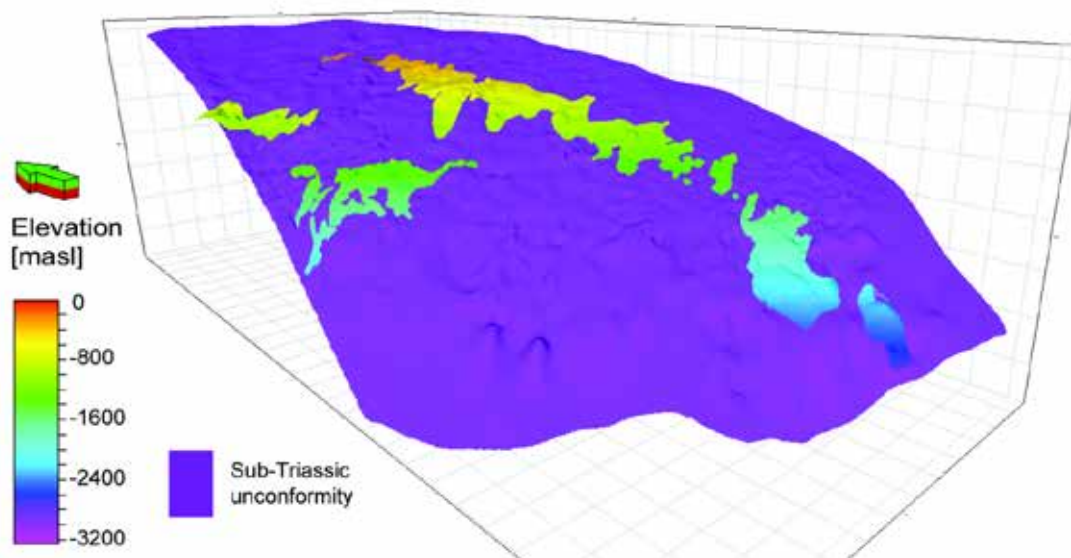


Figure 18: Isometric view of the modelled CDMM and turbidite top surface. The sub-Triassic unconformity surface (purple) is shown for spatial reference. Vertical exaggeration is 50 times.

Table 1: A summary of the interpolation details for the modelled surfaces.

Surface	Count of Stratigraphic Picks	Interpolation Method	Manipulations
Sub-Triassic unconformity	4006	Convergent interpolation	
Montney Formation top	6698	Conformal gridding (to sub-Triassic)	Not below modelled sub-Triassic unconformity Not below CDMM top picks
CDMM base	758	Conformal gridding (to sub-Triassic)	Not below modelled sub-Triassic unconformity Not above modelled Montney Formation top
CDMM top	752	Conformal gridding (to base CDMM)	Not below modelled CDMM base Not above modelled Montney Formation top
Base of turbidites	556	Conformal gridding (to sub-Triassic)	
Top of turbidites	557	Conformal gridding (to base turbidites)	Not below base of turbidites

5.4 Input Surface Uncertainty

Uncertainty analysis was completed for the Montney Formation top and sub-Triassic unconformity interpolated surfaces. Global uncertainty was evaluated using root-mean-square-error (RMSE) values from the base-case modelled surfaces, called the reference surfaces. Local uncertainty was characterized by standard deviation maps. See Babakhani (2016) for details on the method used to calculate the global and local uncertainty for the surfaces.

The mean error for the Montney surface is 0.015 m, suggesting that the interpolated surface is unbiased relative to the reference surface. This means that on average the surface is neither too high nor too low. The RMSE is 2.52 m, meaning about two-thirds of the local errors should be +/- 2.52 m or less from the reference surface. [Figure 19](#) shows a map of the local standard deviation values. Higher values correspond to higher local uncertainty. The greatest uncertainty in the Montney Formation top surface is mostly in areas with relatively little data coverage and at the far northern tip of the model area where there is uncertainty in the projected trend of the Montney.

The mean error for the sub-Triassic unconformity surface is 0.080 m, suggesting that the interpolated surface is unbiased relative to the reference surface. The RMSE is 2.21 m, meaning about two-thirds of the local errors should be +/- 2.21 m or less from the reference surface. [Figure 20](#) shows a map of the local standard deviation values. Higher values correspond to higher local uncertainty. The greatest uncertainty in the sub-Triassic unconformity surface is mostly in areas with relatively little data coverage

at the northeastern and southwestern edges of the model area where the projected trend has the greatest uncertainty.

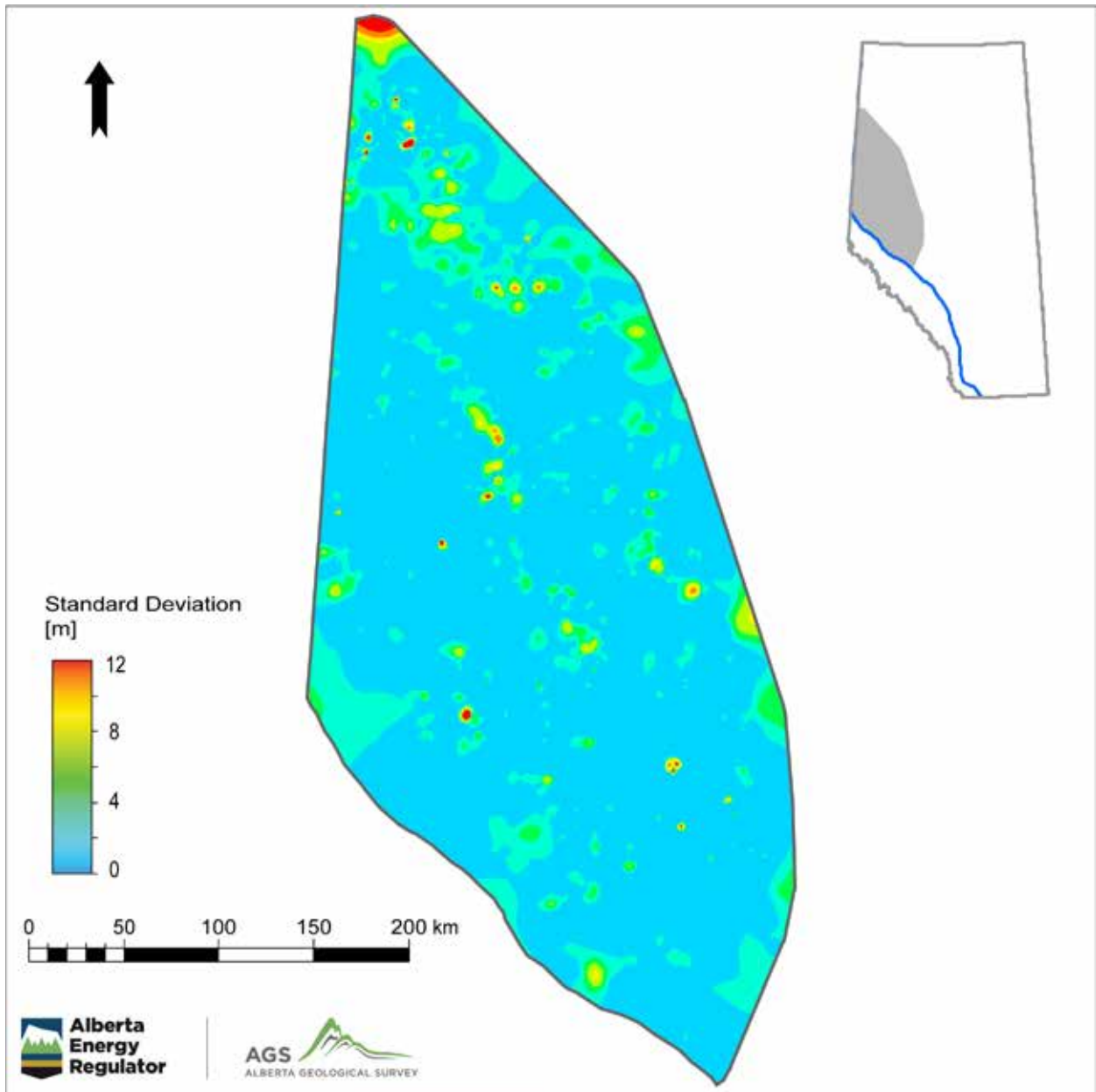


Figure 19: Standard deviation map of the modelled Montney Formation top surface.

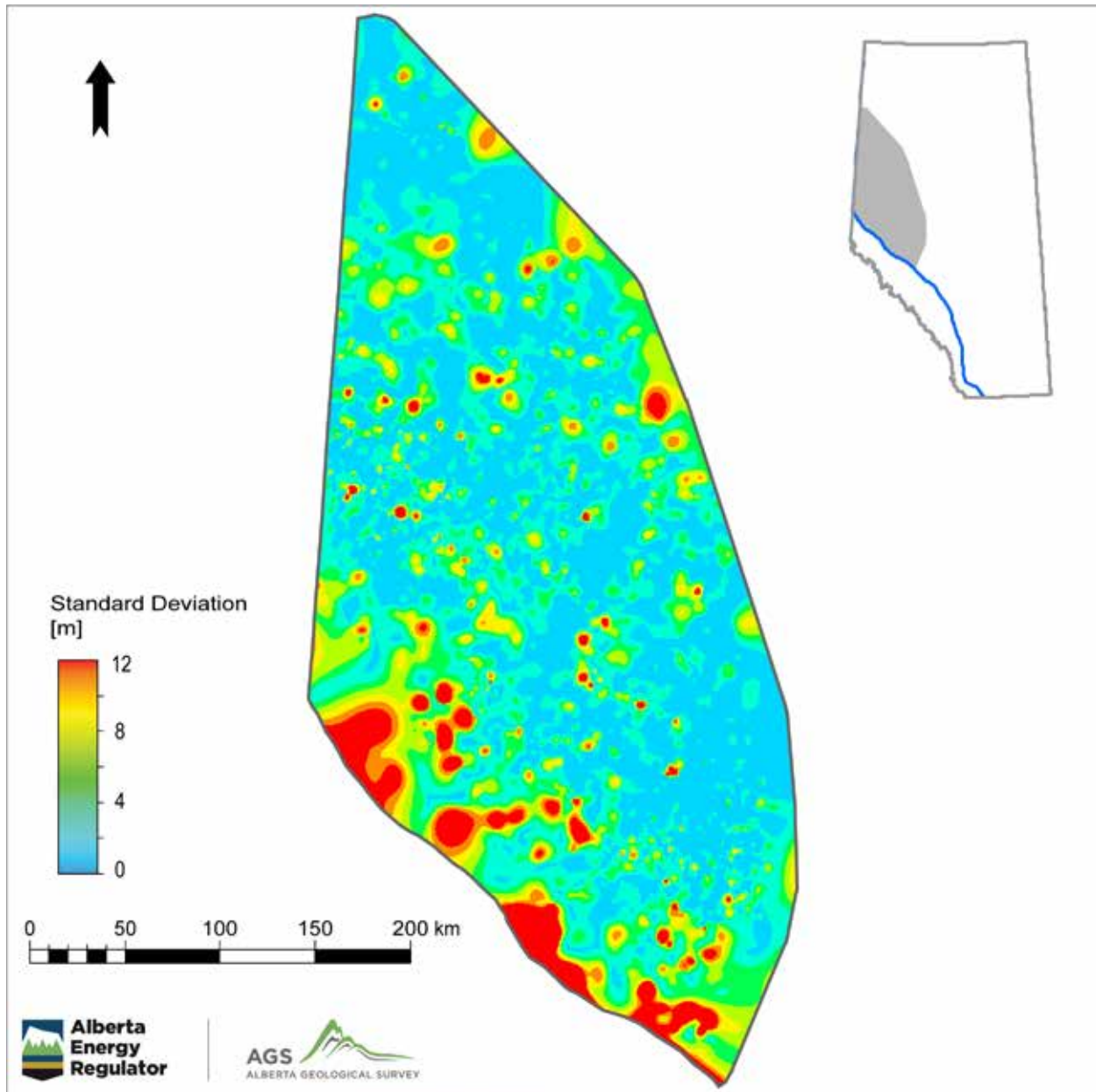


Figure 20: Standard deviation map of the modelled sub-Triassic unconformity modelled surface.

6 Model Construction

The 3D property model of the Montney Formation was built in Petrel using the 3D Pillar Grid tool. The entire Montney Formation was modelled as a single zone due to the lack of information on the Smithian-Dienerian (top of lower Montney) surface. The model was created in several parts, each dealing with a different aspect of the 3D geocellular model:

- A structural/stratigraphic model that defines the 3D volume occupied by the 3D geocellular grid (see Section 6.1).
- A facies model that accounts for the differences between the siltstone that makes up most of the

Montney; the CDMM; and the turbidites (see Section 6.2).

- A 3D property model of the well-log properties (see Section 6.3).
- A 2D property model that was created with only a single layer and then upscaled to the resolution of the 3D property model (see Section 6.4).

6.1 Structural Framework

The structural framework of the model was created using the 3D pillar grid tool. The model extent polygon ([Figure 8](#)) was specified as the geospatial extent of the model domain. The grid increment was set to a cell size of 500 m x 500 m. At this grid increment the model contains 512 x 1124 cells in the XY plane for a total of 575 488 cells, of which 310 136 are active with the rest located outside of the geospatial extent. The model horizons were created using the interpolated Montney Formation top surface and sub-Triassic unconformity surface as inputs.

The structural model was divided into layers to create a 3D geocellular model. The layers are nominally 1 m thick, with some cells being thinner where layers are pinched out by the top model horizon approaching the base model horizon. A minimum cell thickness of 0.5 m was used; any cells below this threshold were merged into the layer below. The layering was done using the “follow base” option, so that the stratigraphic layers follow the sub-Triassic unconformity. The 3D geocellular model contains 512 x 1124 x 329 cells for a total of 189 335 552 grid cells, of which 45 742 140 are active with the rest being outside of the geospatial extents or above the top model horizon.

6.2 Facies Model

The CDMM and turbidites were modelled by using facies rather than zones. This avoids having to model the upper/lower Montney boundary for the areas where the discrete surfaces do not exist and there are no data. Most of the model cells were assigned a facies value of 0, representing siltstone. The cells within the extents of the CDMM and turbidites and between the upper and lower surfaces were assigned values of 1 (CDMM) or 2 (turbidites). Of the 45 742 140 active cells in the model, 213 985 (0.47%) were assigned to the CDMM and 87 677 (0.19%) were assigned to the turbidites. [Figure 21](#) shows isometric views of the facies model. The areas of the CDMM that subcrop at the eroded top of the Montney Formation can be clearly seen in a). Part b) shows an isometric view of the facies model, with the siltstone removed to show the turbidites and western parts of the CDMM.

6.3 3D Property Model

The variables discussed in Section 5.1.3 were simulated in the 3D geocellular model built within the 3D structural framework. The gamma ray, porosity, and TOC variables were modelled using geostatistical methods in a workflow as follows:

- 1) Upscale the gamma-ray, total porosity, and calculated TOC well-log data to the scale of the 3D geocellular grid.
- 2) Transform the data to a normal score distribution with a mean of zero and a variance of one.
- 3) Calculate the experimental variograms for each variable in major and minor horizontal directions, and the vertical direction.
- 4) Fit variogram models to the experimental variograms.

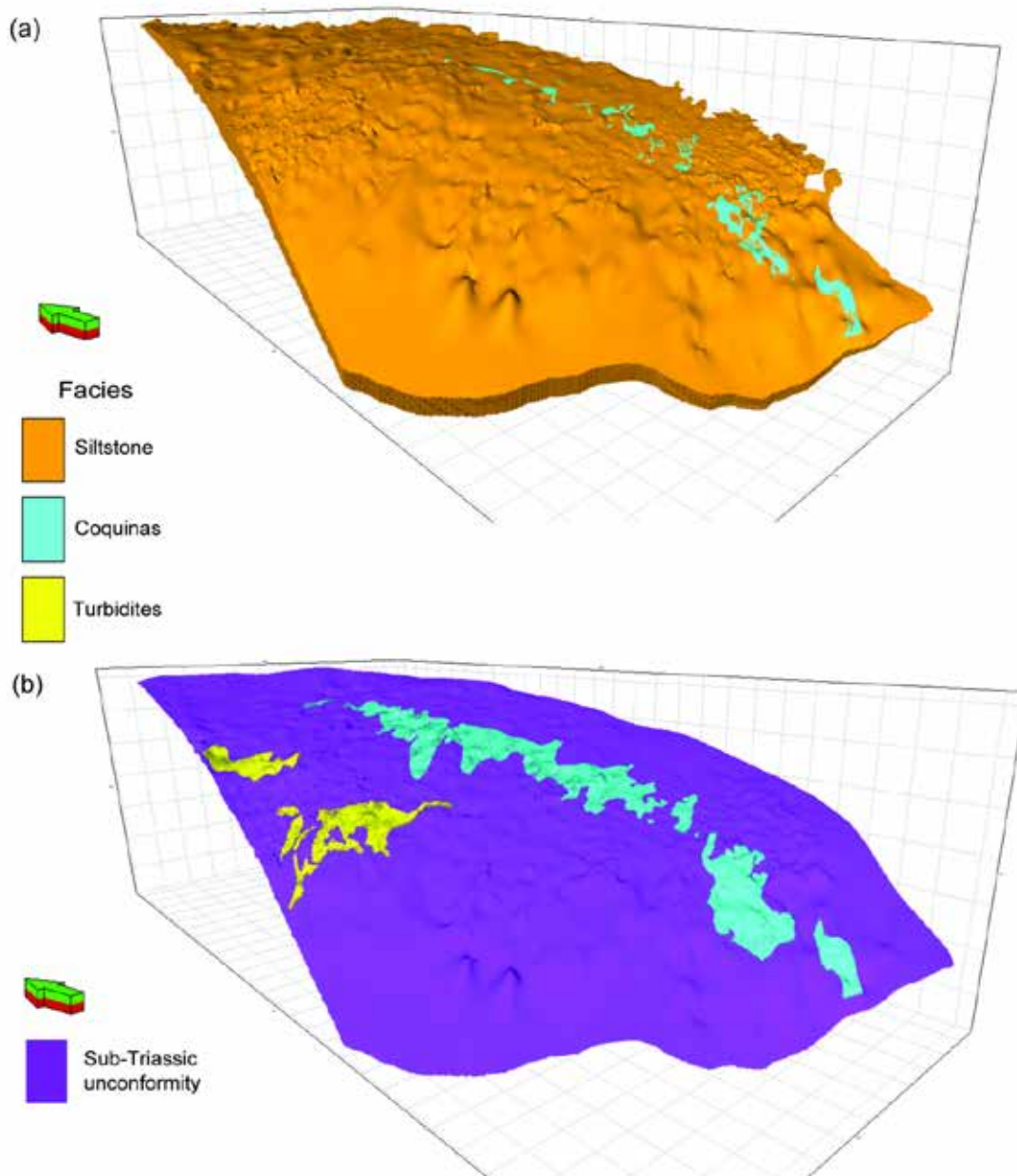


Figure 21: Isometric view of the facies model. a) All facies are shown; the turbidites are hidden by the siltstone. b) Siltstone removed. Vertical exaggeration is 50 times.

- 5) Define the parameters for data searching and the simulation algorithm.
- 6) Populate every cell in the 3D model with a value from the simulation algorithm.
- 7) Repeat the simulation 100 times to capture the full range of uncertainty.

6.3.1 Upscale Well-Log Data

The well-log data discussed in Section 5.1.3 are recorded at very fine regular intervals (typically 6” or 15.2 cm). This fine of a scale of data is both impractical to model directly and inapplicable to a 3D model where the cells are 500 x 500 x 1 m. The data were upscaled from the well logs to the geocellular model to facilitate the property modelling. The averaging of a data set from a scale of 15.2 cm to 1 m reduces the variance of the data distribution as some of the highest and lowest values are smoothed out. This is a well-accepted property of upscaling and does not impact the quality of the final model.

The 6513 gamma-ray well logs were upscaled and the values were assigned to 353 847 cells in the geocellular model. [Figure 22](#) shows an isometric view of the upscaled cells.

The 534 porosity well logs were upscaled and the values were assigned to 63 986 cells in the geocellular model. [Figure 23](#) shows an isometric view of the upscaled cells.

The 534 TOC well logs were upscaled and the values were assigned to 71 795 cells in the geocellular model. [Figure 24](#) shows an isometric view of the upscaled cells. There are more TOC upscaled cells than porosity upscaled cells because the TOC logs were used to calculate porosity, so any log readings missing a TOC value also did not have a porosity value.

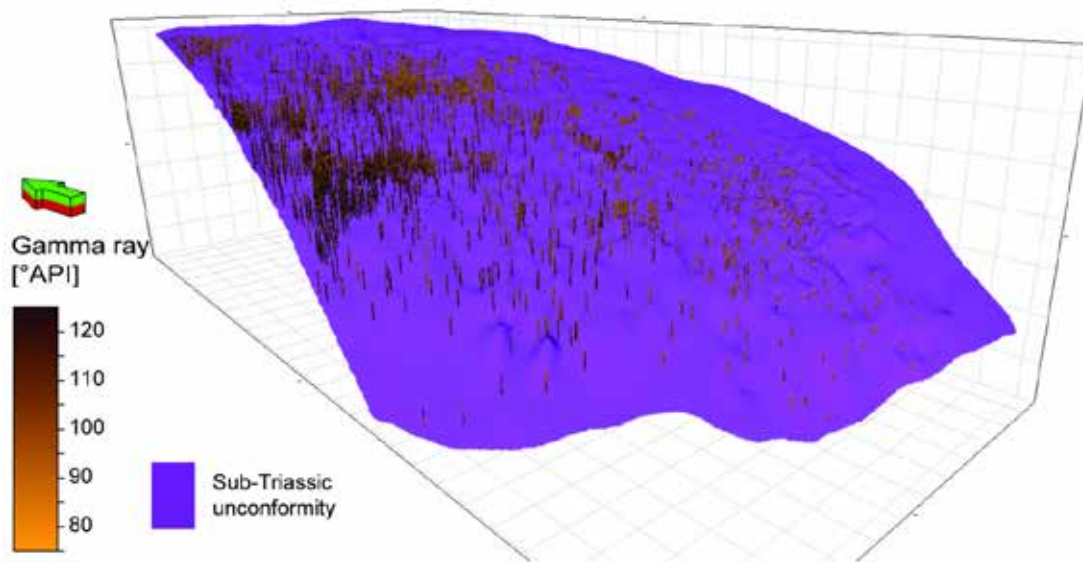


Figure 22: Isometric view of the 353 847 upscaled cells in the gamma-ray model. The sub-Triassic unconformity surface (purple) is shown for spatial reference. Vertical exaggeration is 50 times.

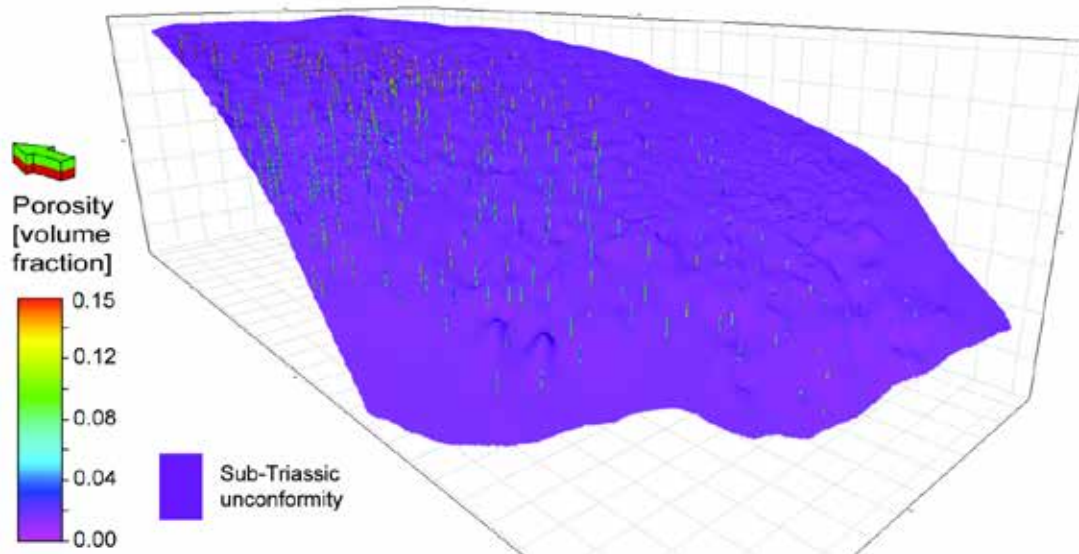


Figure 23: Isometric view of the 63 986 upscaled cells in the porosity model. The sub-Triassic unconformity surface (purple) is shown for spatial reference. Vertical exaggeration is 50 times.

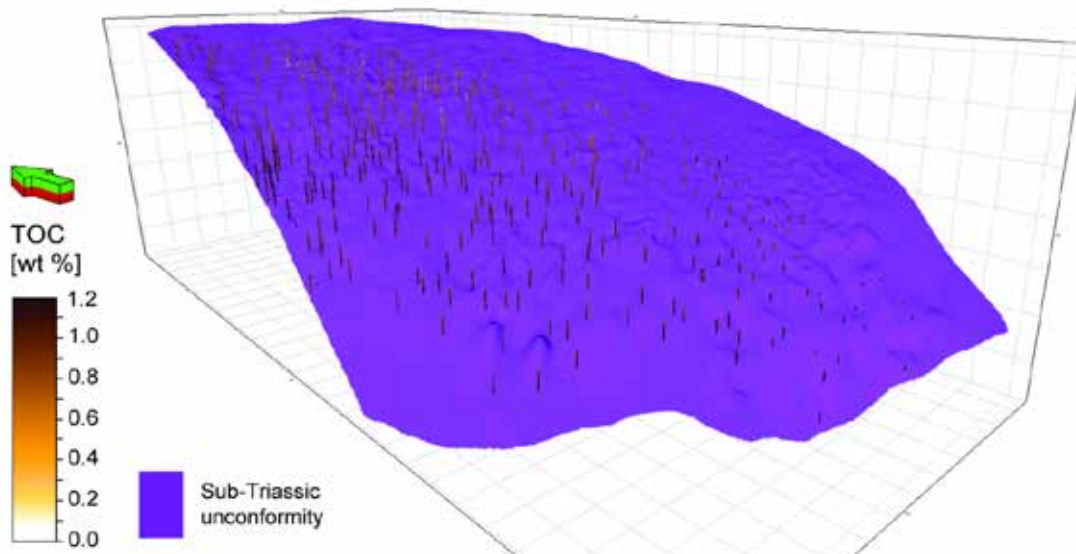


Figure 24: Isometric view of the 71 795 upscaled cells in the TOC model. The sub-Triassic unconformity surface (purple) is shown for spatial reference. Vertical exaggeration is 50 times.

6.3.2 Geostatistical Analysis

The first step towards carrying out a geostatistical simulation is to transform the data to standard normal (Gaussian) distributions. This transformation forces the distribution to have a mean of zero, a variance of

one, and a normal or bell-curve distribution. This distribution has many mathematical properties that make it useful for modelling. The shape and units of the input distribution is restored by applying a back transformation after modelling is completed. For reference, [Table 2](#) shows the minimum, maximum, mean, and standard deviation values for each variable within each facies, before the normal score transformation.

Table 2: Univariate distribution values for the upscaled well-log variables.

Variable	Facies	Minimum	Maximum	Mean	Standard Deviation
Gamma ray	Siltstone	25	175	97.7	23.0
	CDMM	25	175	60.2	34.9
	Turbidites	39.3	175	101.3	19.2
Porosity	Siltstone	0.000	0.391	0.090	0.043
	CDMM	0.008	0.246	0.096	0.039
	Turbidites	0.016	0.180	0.094	0.032
TOC	Siltstone	0.00	2.04	0.68	0.26
	CDMM	0.00	1.35	0.52	0.24
	Turbidites	0.25	1.64	0.90	0.28

The algorithm used for property simulation in Petrel is Gaussian Random Function Simulation (GRFS, Daly et al., 2010). This is a geostatistical method that is based on kriging (Pyrzcz and Deutsch, 2014) to determine interpolated values, and then adds an unconditional simulation to the kriging estimates to simulate a realization conditional to the available data. This method is implemented in Petrel 2015, is computationally efficient, and produces results that are comparable to other geostatistical simulation methods such as sequential Gaussian simulation (SGS; Pyrcz and Deutsch, 2014).

All kriging-based methods require the spatial structure of the modelled variable to be quantified. The spatial structure is represented by a variogram, which is modelled by calculating an experimental variogram that quantifies the difference in values at specified distances, called lags. A variogram is calculated in the major and minor directions of spatial correlation as well as the vertical direction. Each direction is modelled mostly independently of the others, with the weight or sill values of the different model functions being the only interaction between them. For the gamma-ray, porosity, and TOC variables in all facies, the major direction of horizontal spatial correlation is an azimuth of 150 degrees and the minor direction is perpendicular to that, at an azimuth of 60 degrees. [Figure 25](#) shows the three variogram directions for the gamma-ray variable in the siltstone facies as an example.

Variograms were calculated and modelled for gamma ray, porosity, and TOC in each of the siltstone, CDMM, and turbidite facies. [Table 3](#) shows a summary of the variogram parameters for the gamma-ray variable; [Table 4](#) shows a summary of the variogram parameters for the porosity variable, and [Table 5](#) shows a summary of the variogram parameters for the TOC variable. The normal score transformation is applied to ensure the total sill of each variogram is equal to one.

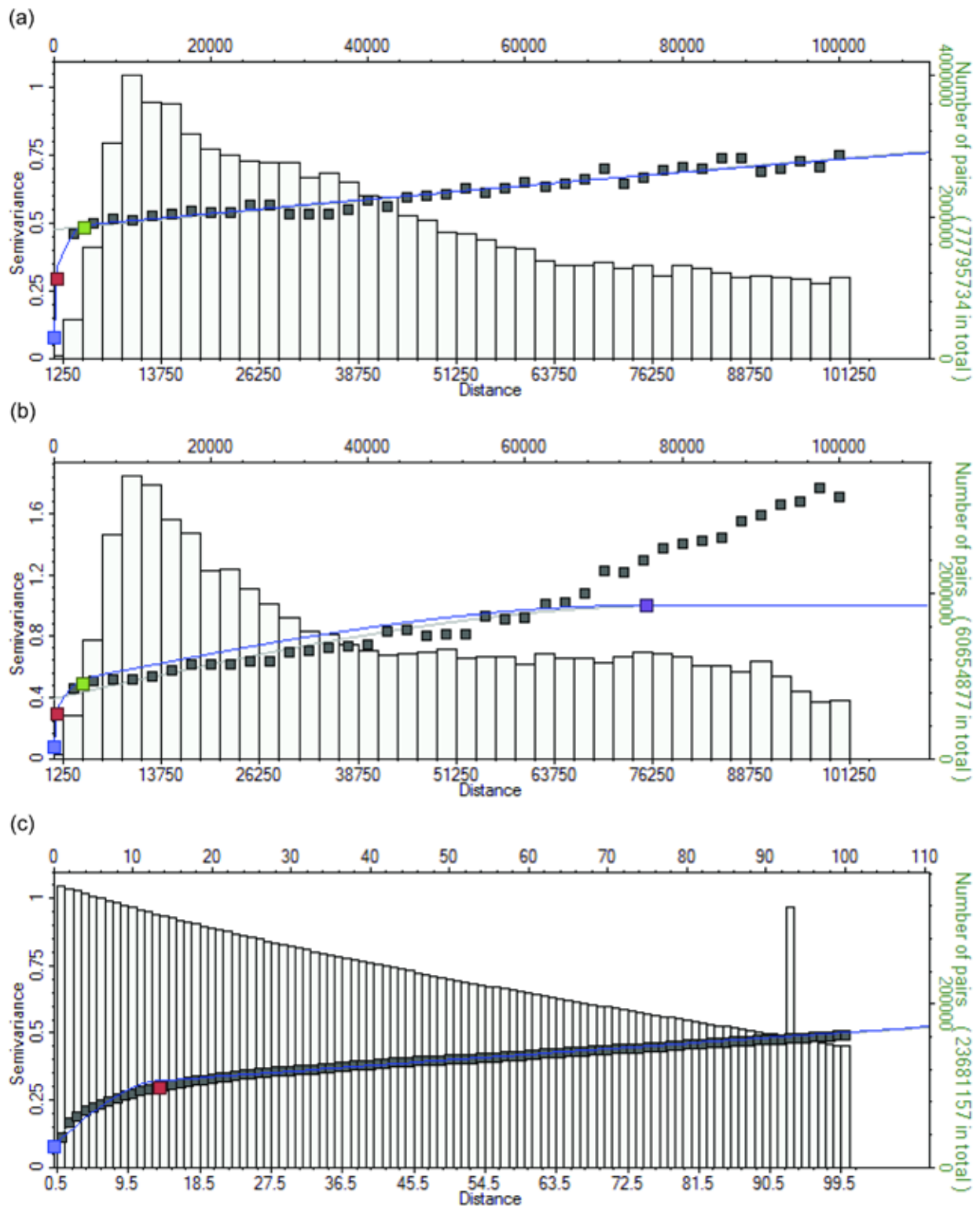


Figure 25: Variogram model in siltstone for the gamma-ray variable in the 3D property model. a) major direction; b) minor direction; c) vertical direction. Grey squares: experimental variograms; grey bars: number of variogram pairs at each lag; blue/grey lines: modelled variogram functions; red/green/purple squares: individual variogram function ranges and sills.

Three model structures were needed to adequately fit the experimental variogram; there are several causes for needing three structures when ideally fewer would be used. The three directions have different apparent nugget effects, making it necessary to use a non-nugget structure to account for this. There is zonal anisotropy, where the variograms do not appear to reach the sill of 1.0 within the search radius; a very long-range structure is used to account for this.

Table 3: Variogram parameters for the gamma-ray variable in the 3D property model.

Variable	Facies	Structure	Type	Sill	Major Range	Minor Range	Vertical Range
Gamma ray	Siltstone	0	Nugget	0.0781			
		1	Spherical	0.2147	536.336	533.719	13.428
		2	Spherical	0.1908	3856.054	3787.542	500
		3	Spherical	0.5164	296814.1	75373.81	500
Gamma ray	CDMM	0	Nugget	0			
		1	Exponential	0.3888	19.956	85.817	3.796
		2	Spherical	0.6111	4731.854	4803.718	29.692
		3	Spherical	0.6111	4731.854	4803.718	29.692
Gamma ray	Turbidites	0	Nugget	0.2672			
		1	Exponential	0.3028	1088.34	1022.307	5.783
		2	Spherical	0.4299	7804.174	7693.42	35.631

Table 4: Variogram parameters for the porosity variable in the 3D property model.

Variable	Facies	Structure	Type	Sill	Major Range	Minor Range	Vertical Range
Porosity	Siltstone	0	Nugget	0.05			
		1	Exponential	0.15	164.357	52.421	6.868
		2	Spherical	0.3	15470.39	14026.65	250
		3	Spherical	0.5	320000	98778.6	250
Porosity	CDMM	0	Nugget	0			
		1	Exponential	0.3	8891.549	8683.835	2.487
		2	Spherical	0.2	27411.53	17329.22	3.103
		3	Spherical	0.5	213211.4	180077.5	80
Porosity	Turbidites	0	Nugget	0.05			
		1	Exponential	0.15	26665.05	27257.72	1.267
		2	Spherical	0.8	30243.37	30537.84	25.529

Table 5: Variogram parameters for the TOC variable in the 3D property model.

Variable	Facies	Structure	Type	Sill	Major Range	Minor Range	Vertical Range
TOC	Siltstone	0	Nugget	0			
		1	Exponential	0.05	500	500	10
		2	Exponential	0.2	66266.12	33591.61	400
		3	Spherical	0.75	300000	78210.98	400
TOC	CDMM	0	Nugget	0			
		1	Exponential	0.1182	500	500	3.228
		2	Spherical	0.8812	33000	33000	75
TOC	Turbidites	0	Nugget	0			
		1	Exponential	0.1182	500	500	3.228
		2	Spherical	0.8812	33000	33000	75

6.3.3 Populate 3D Geocellular Grid

The GRFS method in Petrel was used to simulate 100 realizations of the gamma-ray, total porosity, and TOC variables. The simulation method ensured that every active cell in the 3D grid was assigned a value for every realization. The porosity and TOC variables were populated using cosimulation and the gamma-ray variable as a secondary variable. This accounts for the correlation between the variables and uses the fact that there is much more gamma-ray data than the other variables. The correlation of the normal score transformed variables is -0.18 between gamma ray and porosity; and 0.25 between gamma ray and TOC.

Figure 26 shows isometric views of the gamma-ray model. There are two simulated realizations and the arithmetic mean of 100 realizations. The realizations are different but equally probable to one another. The simulated realizations show the characteristic “patchy” look of a mixture of high and low values. The arithmetic mean of 100 realizations is nearly identical to a kriged model (this is expected) and is therefore too smooth, with cell values tending towards the centre of the distribution and lacking the randomness and variability of real geological data. Figure 27 shows isometric views of the porosity model and Figure 28 shows isometric views of the TOC model.

6.4.2D Property Model

The variables discussed in Section 5.1.4 were simulated in the 3D geocellular model built within the 3D structural framework. The pressure gradient, temperature gradient, gas-oil ratio, and condensate-gas ratio variables were modelled using geostatistical methods. The point property data were first modelled in a simplified 3D grid with a single layer and then upscaled to the same 3D geocellular grid as the 3D property model at a 500 x 500 x 1 m cell size. This simplified 3D grid will be referred to as a 2D grid for clarity. The 2D grid contains 512 x 1124 x 1 cells for a total of 575 488 cells. The workflow is as follows:

- 1) Create a 3D geocellular grid within the structural framework that has a single layer and is effectively a 2D grid.
- 2) Upscale the point property data to the scale of the 2D grid.
- 3) Transform the data to a normal score distribution with a mean of zero and a variance of one.

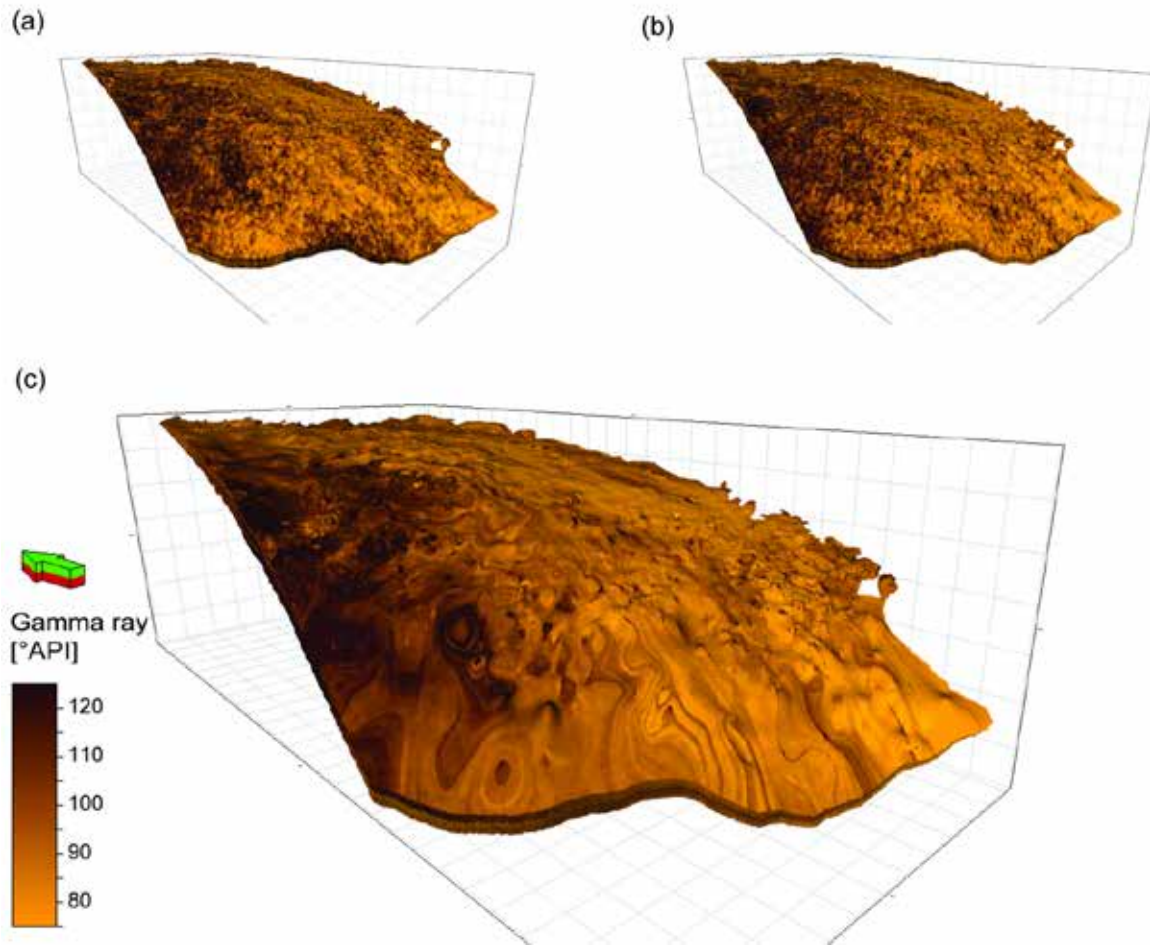


Figure 26: Isometric views of the gamma-ray model. a) and b) two simulated realizations; c) arithmetic mean of 100 realizations. Vertical exaggeration is 50 times.

- 4) Calculate the experimental variograms for each variable in major and minor horizontal directions.
- 5) Fit variogram models to the experimental variograms.
- 6) Define the parameters for data searching and the simulation algorithm.
- 7) Populate every cell in the 2D model with a value from the simulation algorithm.
- 8) Repeat the simulation 100 times to capture the full range of uncertainty.
- 9) Upscale the simulated values from the 2D model to the 3D model.

6.4.1 Upscaled Point Property Data

The point property data values exist in the model as discrete points. To populate the geocellular grid with values, the point values were upscaled to the cells in the 2D grid. The 2D grid was constructed with only a single layer, so all point values within a 500 x 500 m cell were averaged to assign an upscaled value to that cell.

The 2032 pressure gradient data were upscaled to 1752 cells in the 2D grid. [Figure 29](#) shows an isometric view of the upscaled pressure gradient cells.

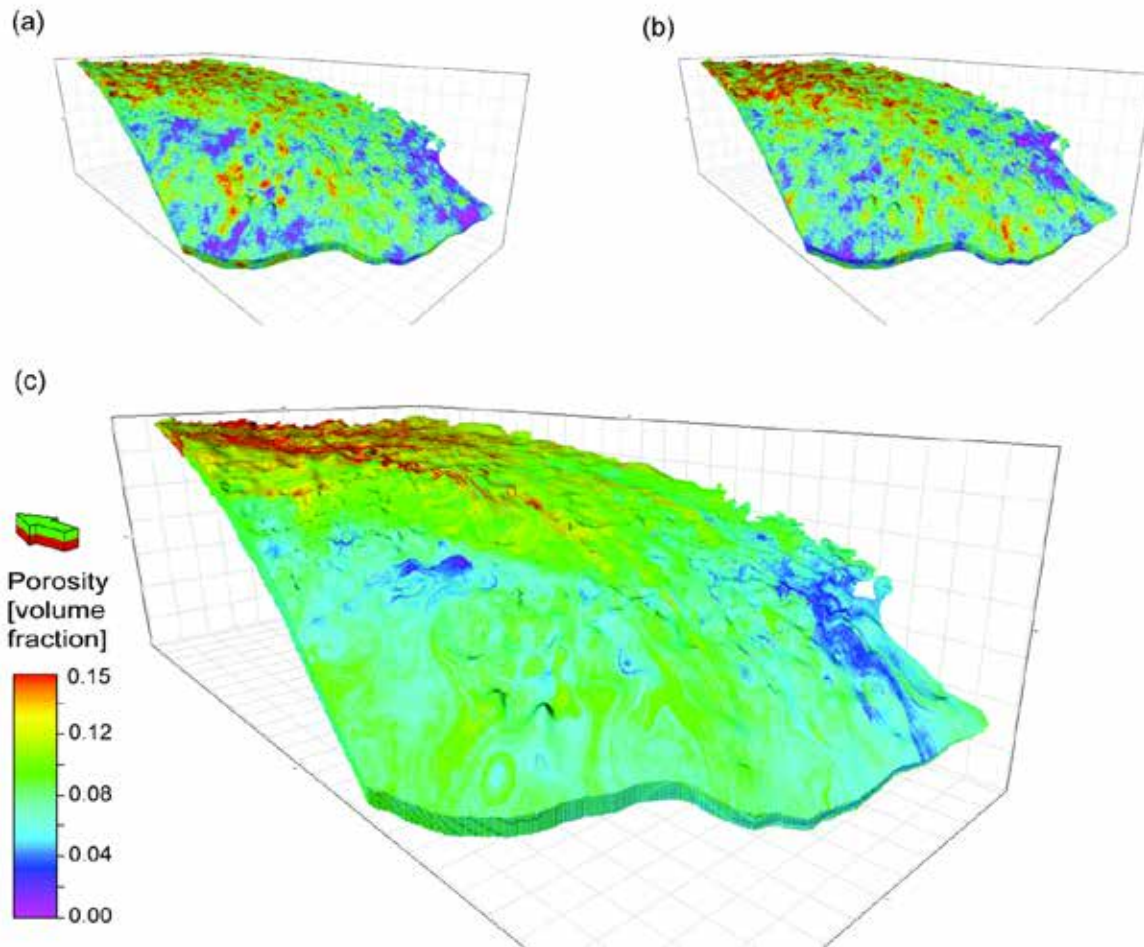


Figure 27: Isometric views of the porosity model. a) and b) two simulated realizations; c) arithmetic mean of 100 realizations. Vertical exaggeration is 50 times.

The 2146 temperature gradient data were upscaled to 1850 cells in the 2D grid. [Figure 30](#) shows an isometric view of the upscaled temperature gradient cells.

The 4804 gas-oil ratio data were upscaled to 3745 cells in the 2D grid. [Figure 31](#) shows an isometric view of the upscaled gas-oil ratio cells.

The 11 260 condensate-gas ratio data were upscaled to 3219 cells in the 2D grid. [Figure 32](#) shows an isometric view of the upscaled condensate-gas ratio cells. The large reduction in the number of data points for the condensate-gas ratio is caused by the number of wells with multiple gas tests that were averaged out in the upscaling process.

6.4.2 Geostatistical Analysis

The 2D simulation was done following the same process used for the 3D variables in Section 6.3.3. The variables were transformed to standard normal distributions; the variograms were modelled; GRFS was used to populate the 2D grid; and the simulated values were back transformed to the original distributions. [Table 6](#) shows the minimum, maximum, mean, and standard deviation of the upscaled point property

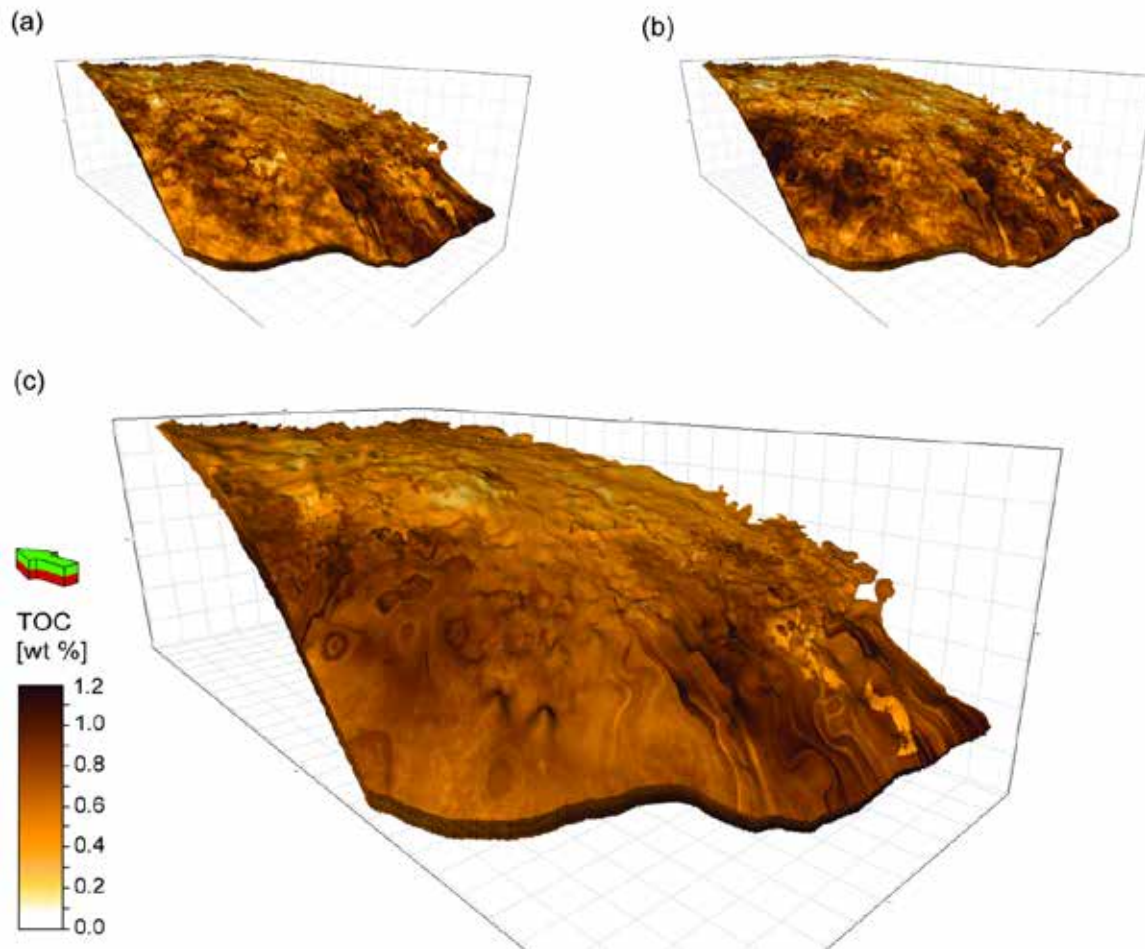


Figure 28: Isometric views of the TOC model. a) and b) two simulated realizations; c) arithmetic mean of 100 realizations. Vertical exaggeration is 50 times.

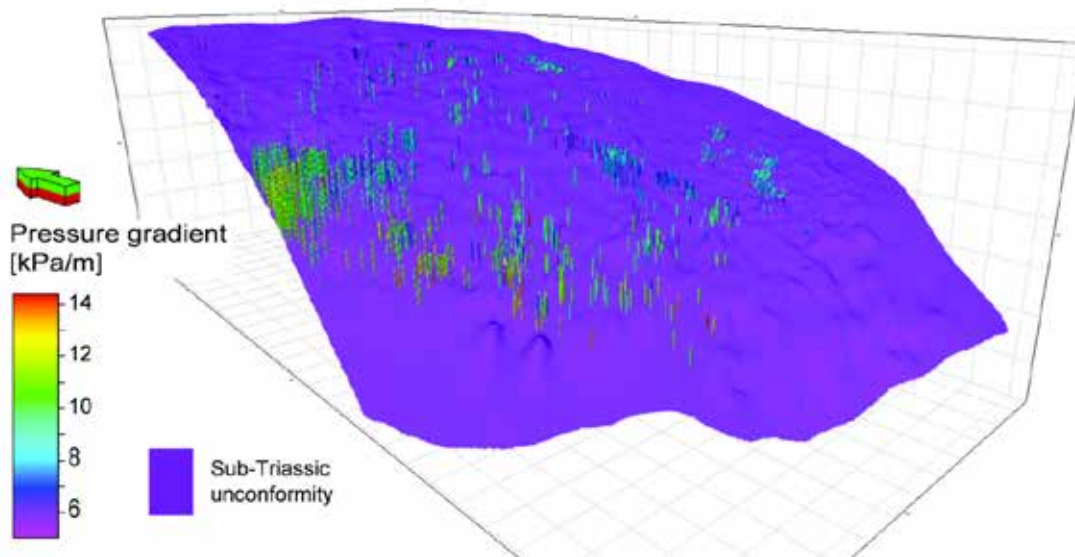


Figure 29: Isometric view of the 1752 upscaled cells in the pressure gradient model. The sub-Triassic unconformity surface (purple) is shown for spatial reference. Vertical exaggeration is 50 times.

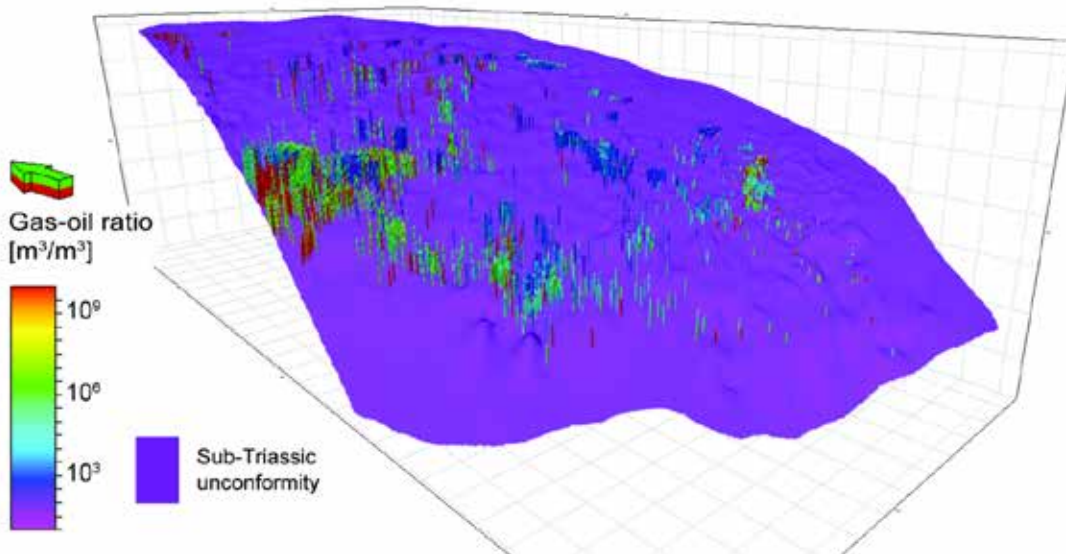


Figure 30: Isometric view of the 1850 upscaled cells in the temperature gradient model. The sub-Triassic unconformity surface (purple) is shown for spatial reference. Vertical exaggeration is 50 times.

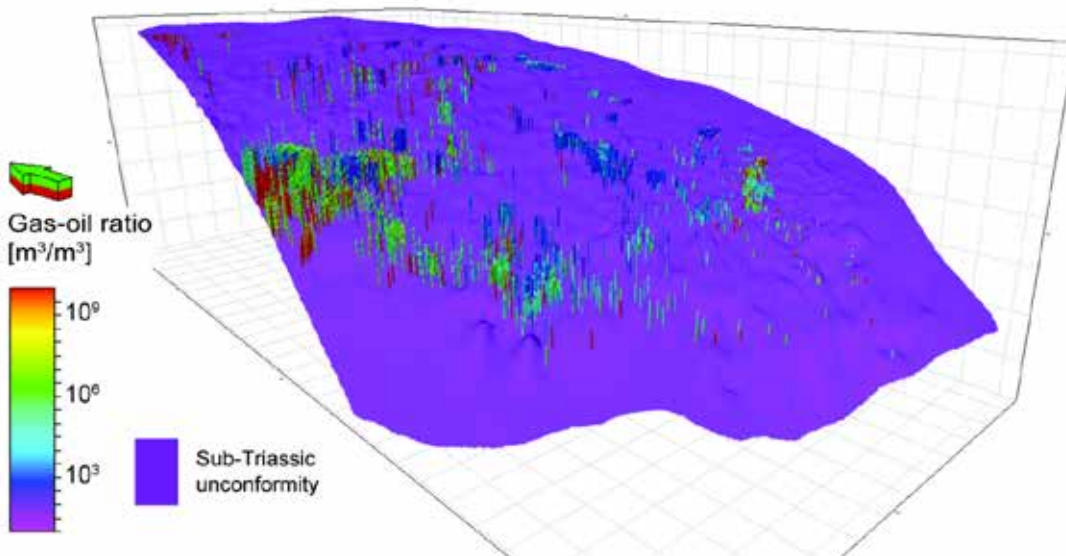


Figure 31: Isometric view of the 3745 upscaled cells in the gas-oil ratio model. The sub-Triassic unconformity surface (purple) is shown for spatial reference. Vertical exaggeration is 50 times.

variables before the normal score transformation, for reference. The entire 3D model was made as one layer in the 2D grid and so there is no separation of different facies in the 2D model.

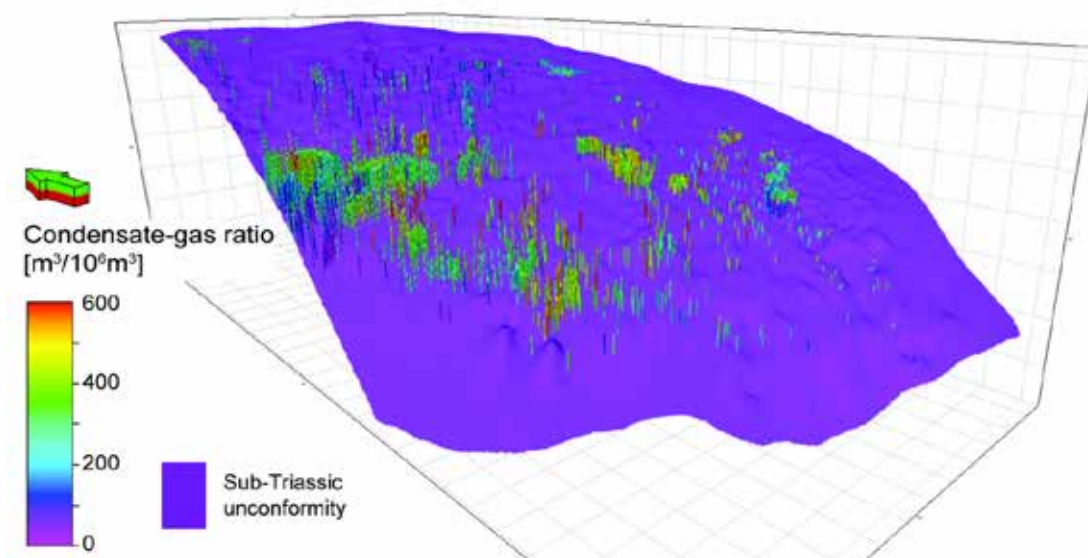


Figure 32: Isometric view of the 3219 upscaled cells in the condensate-gas ratio model. The sub-Triassic unconformity surface (purple) is shown for spatial reference. Vertical exaggeration is 50 times.

Table 6: Univariate distribution values for the upscaled point property variables. Mean refers to the arithmetic mean except for gas-oil ratio, which is the geometric mean*.

Variable	Minimum	Maximum	Mean	Standard Deviation
Pressure gradient (kPa/m)	5.0	14.4	8.7	1.8
Temperature gradient (°C/km)	24.7	43.9	33.0	2.6
Gas-oil ratio	17	1.0×10^{10}	97,470*	
Condensate-gas ratio	0	744	319	141

Variograms were calculated and modelled for the pressure gradient, temperature gradient, gas-oil ratio, and condensate-gas ratio variables. [Figure 33](#) shows the major and minor variogram directions for the pressure gradient variable as an example. There is no vertical direction because there is only a single layer in the 2D grid. [Table 7](#) shows the parameters for all of the variograms for the 2D variables, which were the parameters used to create the model.

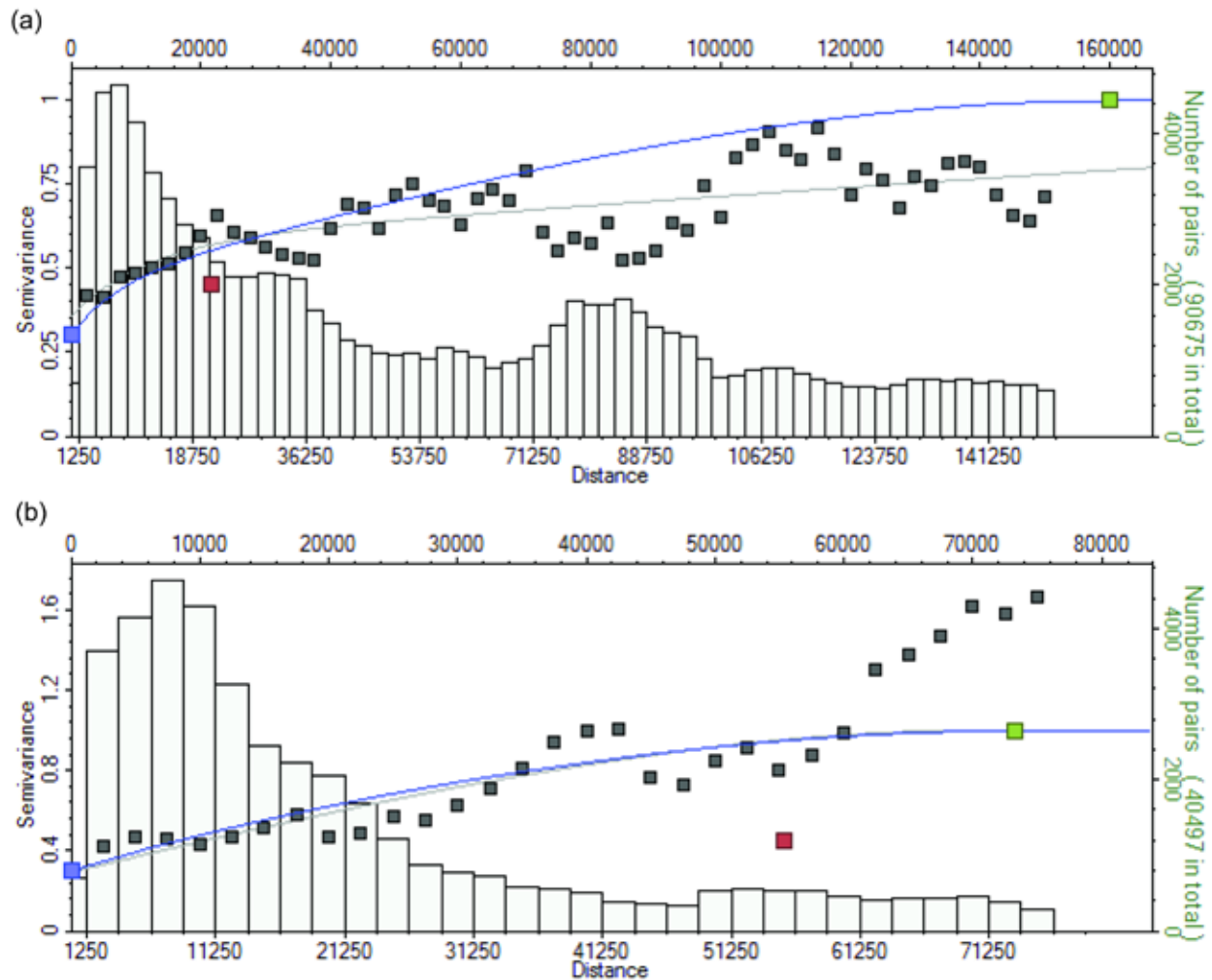


Figure 33: Variogram model for the pressure gradient variable in the 2D property model. a) major direction; b) minor direction. Grey squares: experimental variograms; grey bars: number of variogram pairs at each lag; blue/grey lines: modelled variogram functions; red/green squares: individual variogram function ranges and sills.

Table 7: Variogram parameters for the variables in the 2D property model.

Variable	Structure	Type	Sill	Major Range	Minor Range
Pressure gradient	0	Nugget	0.3		
	1	Exponential	0.15	21650.94	55336.53
	2	Spherical	0.55	160000	73221.32
Temperature gradient	0	Nugget	0.15		
	1	Exponential	0.3	21497.16	48075.11
	2	Spherical	0.55	120000	50762.41
Gas-oil ratio	0	Nugget	0.2		
	1	Spherical	0.5	22758.85	17010.67
	2	Spherical	0.3	120000	100000

Condensate-gas ratio	0	Nugget	0.16		
	1	Exponential	0.3	35348.16	17362.39
	2	Spherical	0.54	89796.42	57408.64

6.4.3 Populate 2D Geocellular Grid

The GRFS method in Petrel was used to simulate 100 realizations of the pressure gradient, temperature gradient, gas-oil ratio, and condensate-gas ratio variables. Every cell in the 2D grid was assigned a value for each realization. [Figure 34](#) shows isometric views of the simulated pressure gradient variable. There are two realizations and the arithmetic mean of 100 realizations. [Figure 35](#) shows isometric views of the simulated temperature gradient variable.

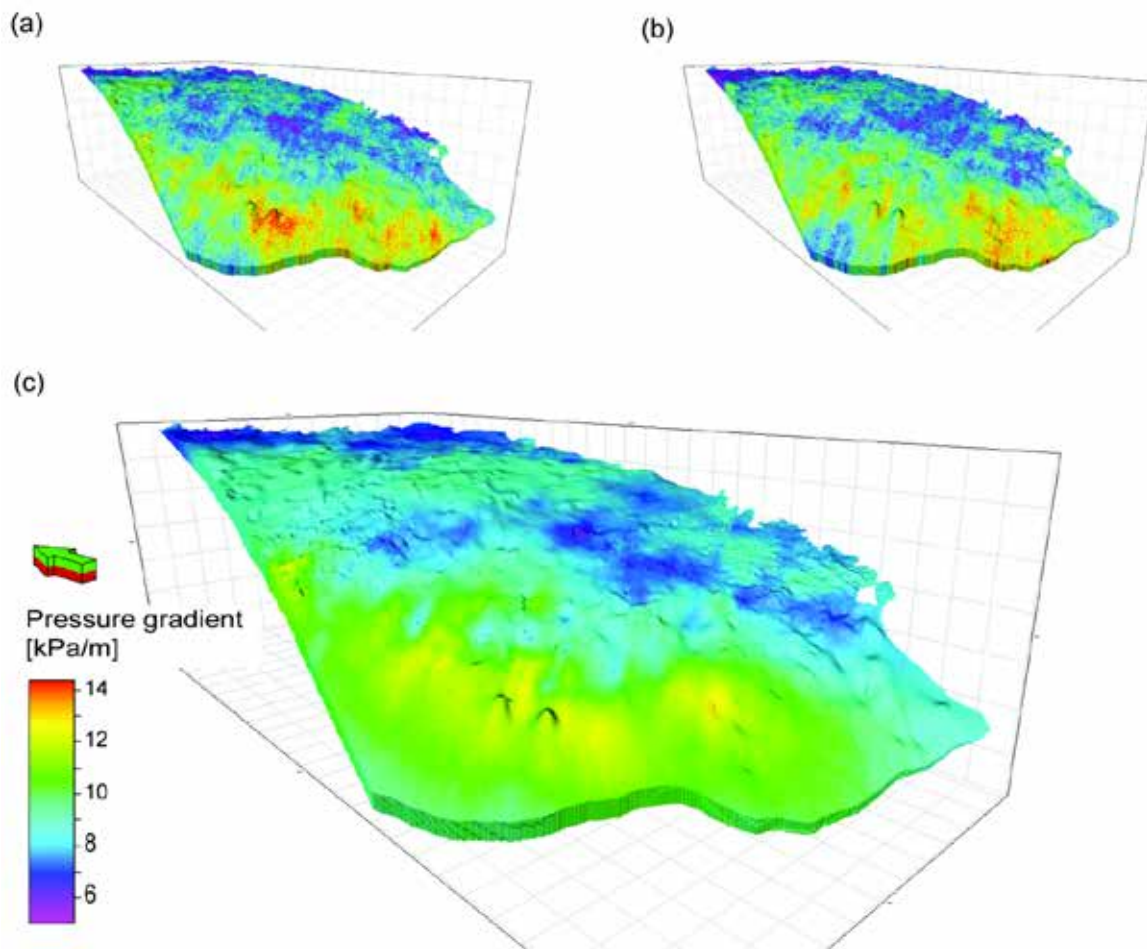


Figure 34: Isometric views of the pressure gradient model. a) and b) two simulated realizations; c) arithmetic mean of 100 realizations. Vertical exaggeration is 50 times.

[Figure 36](#) shows isometric views of the gas-oil ratio variable. There are two realizations and the geometric mean of 100 realizations. The geometric mean was used for gas-oil ratio because of the lognormal nature of the distribution; the highest values are orders of magnitude greater than the low end of the distribution. [Figure 37](#) shows isometric views of the simulated condensate-gas ratio variable.

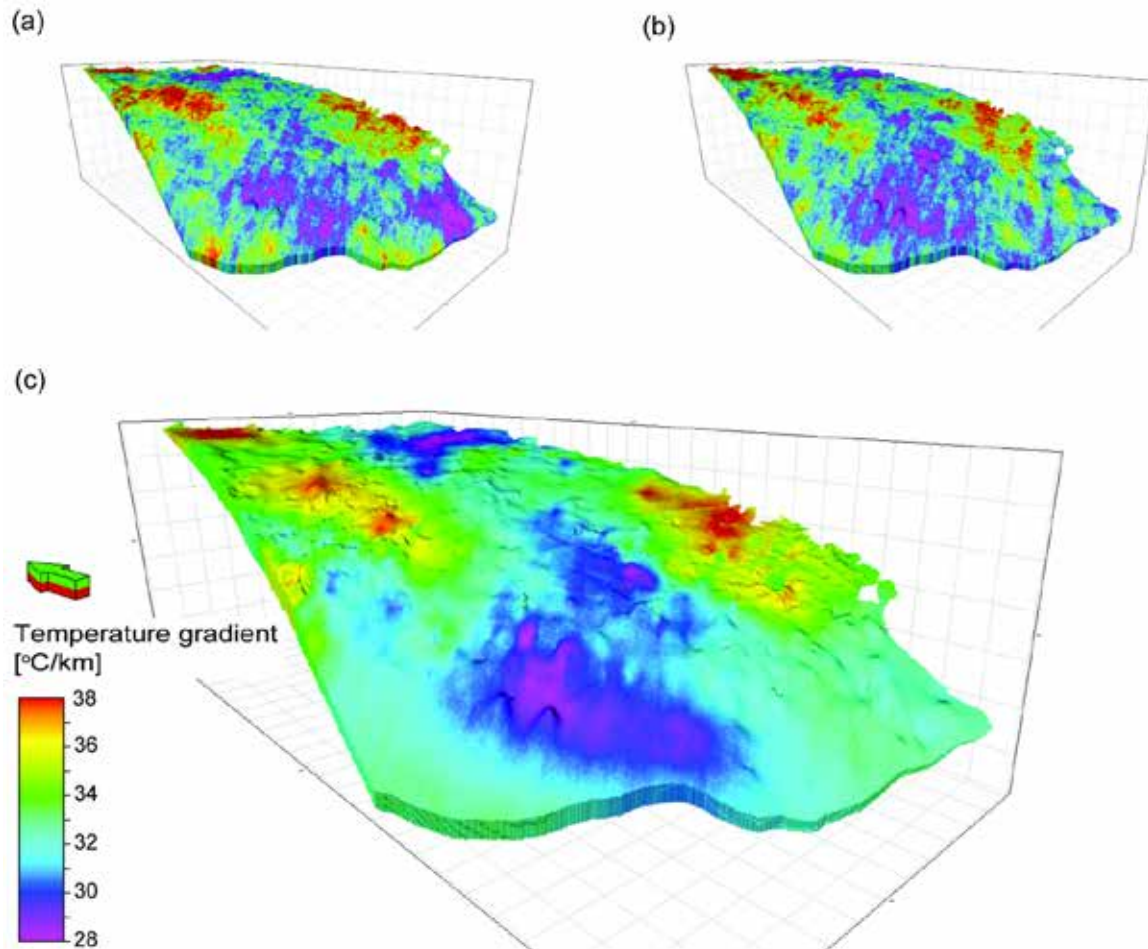


Figure 35: Isometric views of the temperature gradient model. a) and (b) two simulated realizations; c) arithmetic mean of 100 realizations. Vertical exaggeration is 50 times.

6.4.4 Upscaling to the 3D Grid

The simulated realizations in the 2D grid were upscaled to the 3D grid to allow for calculations using all of the variables in a single workflow. The upscaling assigns the single 2D value at each (x,y) location to all of the layers in the 3D grid.

7 Model Outputs

This section describes the post-construction part of the geomodelling workflow (Part 6) after the 3D model construction was finalized. This section describes how the model and components of the model are disseminated to the end user without the need for Petrel software. Digital data outputs generated from the 3D model include model tabular point data, model extents, discrete and continuous model horizons, property data as ASCII points, and model surfaces in iMOD format (see Section 3 for definitions).

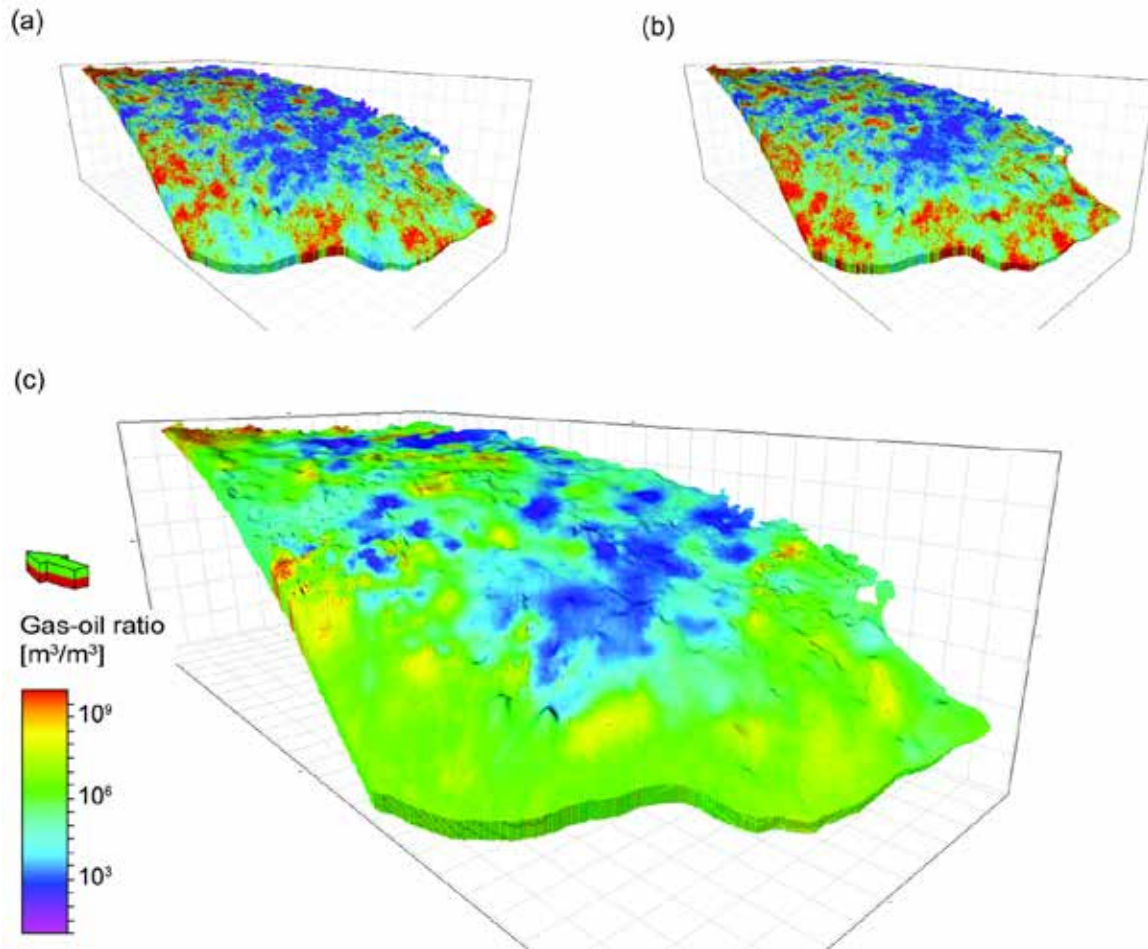


Figure 36: Isometric views of the gas-oil ratio model. a) and b) two simulated realizations; c) geometric mean of 100 realizations. Vertical exaggeration is 50 times.

7.1 Digital Data

The Montney 3D model was deconstructed to provide digital data in a standard format to the stakeholder. This allows the end user to download the information they are interested in or to re-construct the model in accordance with the methodology outlined in this report.

There are four digital data deconstructed model outputs from the Montney 3D model available in standard formats:

- **Model extents:** zone model extents published as GIS data polygon features
- **Model horizons (discrete):** discrete model horizons published as gridded data in ASCII format
- **Model horizons (continuous):** continuous model horizons published as gridded data in ASCII format for use with iMOD 3D visualization (see Section 7.2)
- **Model properties:** populated model property of facies, and/or 3D or 2D properties (mean of 100 realizations and standard deviation) as point data in ASCII format and Petrel format.

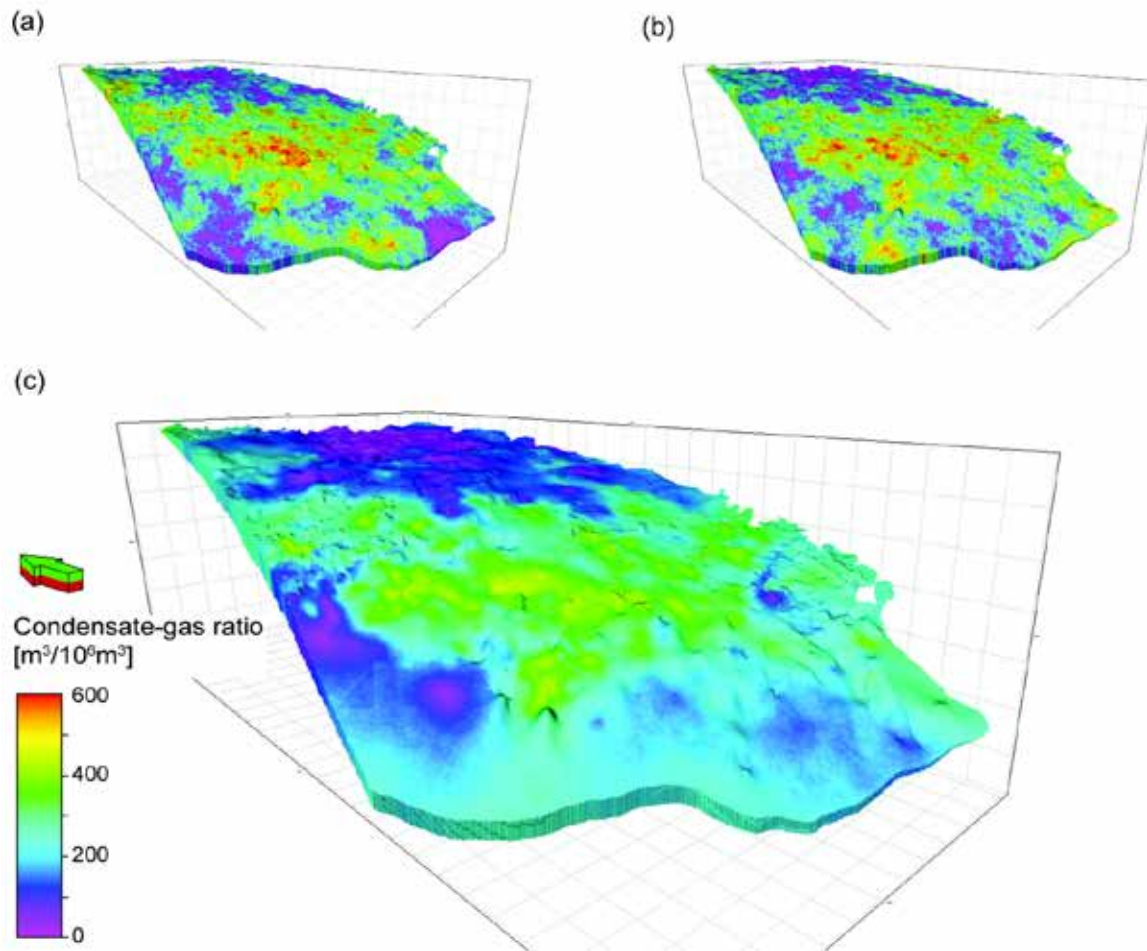


Figure 37: Isometric views of the condensate-gas ratio model. a) and b) two simulated realizations; c) arithmetic mean of 100 realizations. Vertical exaggeration is 50 times.

7.2 iMOD 3D Visualization

Visualization of the 3D model can be done in iMOD, an open source 3D digital data viewing software available for download from Deltares (<https://oss.deltares.nl/web/imod/>). All deconstructed model digital data can be viewed in 2D and 3D (model tabular point data, extents, and horizons). In this software, 3D models can be rotated, toggled on and off, or exploded for viewing. Additional functionality of iMOD includes the ability to create cross-sections and clip the model using an intersection plane. The user can import any data into the model domain and visualize how it relates to the zones within the 3D model.

8 Model Quality

The qualitative assessment provides a confidence level (low to high) for each model horizon and property based on three quality categories (Branscombe et al., 2018a): 1) data quality, 2) data quantity, and 3) trueness to geological complexity (for horizons) or trueness to reality (for properties). [Table 8](#) shows a summary of the confidence level for all of the horizons, and [Table 9](#) shows a summary of the confidence level for all of the properties. All categories are scored between 1 and 3 (1 = low; 2 = medium; and 3 = high). For each model horizon or property the categories are added to a maximum of 9. Confidence

levels are determined based on the total score range with: 3–4 = low; 5–7 = medium; and 8–9 = high. Model horizon quality ranges from medium to high. Model property quality ranges from medium to high. Higher confidence levels were influenced by abundant data and if the model property provided an accurate representation of the ground truth.

The data used to produce the model horizons was created and verified by AGS geologists and is all of high quality. The CDMM and turbidites have not been explored fully and the outlines used in the model are preliminary; for this reason, the data quantity is only medium for the top and base model horizons of these geological bodies. The turbidites are not a single continuous unit, and there are a number of turbidites at different stratigraphic levels. Several of them are at the Dienerian-Smithian boundary, but there are others that are not and it is not always obvious to tell them apart. The trueness to geological complexity value was lowered for the turbidites for this reason.

The 3D well log data was calibrated to core data and is of relatively high quality. The gamma-ray values were not normalized. This avoids smoothing out the local variations in the lithology that could be lost when normalization is applied to a large area. A possible variation in the baseline gamma-ray response is the reason for reducing the trueness to reality for the gamma-ray property. The porosity logs used a single grain density across the entire Montney Formation, which is greatly simplified but is the closest assumption that was possible for a large-scale model. The TOC data were calibrated to lab samples but the methodology used has notable variation over a large area. The numerous gamma-ray logs make the data quantity less of a concern for that variable. The limited porosity and TOC logs that were available, due to the more in-depth log analysis necessary, reduce the confidence due to quantity.

The point property data are of lower quality because of the greater uncertainty in the data values and the imprecision of some of the tests used to quantify the properties. There is sufficient quantity of data in the Montney to have high confidence in the spatial data coverage. The trueness to reality is only medium quality due to the assumption that the points are representative of the entire thickness of the model.

Table 8: Confidence level of all modelled horizons.

Model Horizon	Data Quality	Data Quantity	Trueness to Geological Complexity	Model Horizon Confidence Level	
Montney Formation top	3	3	3	9	High
Sub-Triassic unconformity	3	3	3	9	High
CDMM top	3	2	3	8	High
CDMM base	3	2	3	8	High
Top of turbidites	3	2	2	7	Medium
Base of turbidites	3	2	2	7	Medium

Table 9: Confidence level of all modelled properties.

Model Property	Data Quality	Data Quantity	Trueness to Reality	Model Property Confidence Level	
Gamma ray	3	3	2	8	High
Porosity	3	2	2	7	High
TOC	3	2	2	7	Medium
Pressure gradient	2	3	2	7	Medium
Temperature gradient	2	3	2	7	Medium
Gas-oil ratio	2	3	2	7	Medium
Condensate-gas ratio	2	3	2	7	Medium

9 Summary

This work summarizes the methodology used to create a 3D property model of the Montney Formation. The current state of the data is presented and limitations are discussed. All relevant parameters necessary to replicate the property model are specified. The components of the models are available in digital data format.

A variety of data sources were used to carry out this work, including geological interpretations, well logs, well tests, well-production histories, and produced-gas tests. The geological interpretations and picks were used to develop the stratigraphic framework of the model. Well logs were used to model petrophysical properties in 3D. Other data types are represented as discrete points and were used to model reservoir properties in 2D. The 2D model was upscaled to match the 3D geocellular grid. All properties were simulated using GRFS to create 100 realizations that represent the range of uncertainty.

A simplified stratigraphic framework was used for this version of the 3D property model of the Montney Formation, with the possibility of adding further complexity in the future. The properties that were modelled are those necessary to carry out resource calculations. If other data types become available such as newly processed well logs that represent different petrophysical properties, this same methodology can be applied to better represent the complexity of the subsurface and improve the current predictions.

10 References

- Alberta Energy (undated): Deeper rights reversion zone designation lookup; Alberta Energy, URL <https://www.energy.alberta.ca/AU/Services/Pages/DeeperRights.aspx> [October 2018].
- Armitage, J.H. (1962): Triassic oil and gas occurrences in northeastern British Columbia; *Journal of the Alberta Society of Petroleum Geologists*, v. 10, p. 35–36.
- Babakhani, M. (2016): Uncertainty analysis in geological surface modelling; AAPG Annual Convention and Exhibition, Calgary, Alberta, Canada, June 19–22, 2016.
- Branscombe, P., MacCormack, K.E. and Babakhani, M. (2018a): 3D Provincial Geological Framework Model of Alberta, Version 1 – methodology; Alberta Energy Regulator, AER/AGS Open File Report 2017-09, 25 p, URL https://www.ags.aer.ca/publications/OFR_2017_09.html [October 2018]
- Branscombe, P., MacCormack, K.E., Corlett, H., Hathway, B., Hauck, T.E. and Peterson, J.T. (2018b): 3D Provincial Geological Framework Model of Alberta, Version 1 (dataset, multiple files); Alberta Energy Regulator, AER/AGS Model 2017-03, URL https://www.ags.aer.ca/data-maps-models/3D_PGF_model_v1.html [October 2018]
- Daly, C., Quental, S. and Novak, D. (2010): A faster, more accurate Gaussian simulation; GeoCanada Conference, Calgary, AB, Canada, p. 10–14.
- Davies, G. R., Moslow, T.F. and Sherwin, M.D. (1997): The lower Triassic Montney formation, west-central Alberta; *Bulletin of Canadian Petroleum Geology*, v. 45, no. 4, p. 474–505.
- Davies, G.R., Watson, N., Moslow, T.F. and MacEachern, J.A. (2018): Regional subdivisions, sequences, correlations and facies relationships of the Lower Triassic Montney Formation, west-central Alberta to northeastern British Columbia, Canada — with emphasis on role of paleostructure; *Bulletin of Canadian Petroleum Geology*, v. 66, no.1, p. 23–92.
- Edwards, D.E., Barclay, J.E., Gibson, D.W., Kvill, G.E. and Halton, E. (1994): Triassic strata of the Western Canada Sedimentary Basin; *in* Geological Atlas of the Western Canada Sedimentary Basin, Canadian Society of Petroleum Geologists and Alberta Research Council, G.D. Mossop and I. Shetsen (ed.), URL <https://www.ags.aer.ca/publications/chapter-16-triassic-strata> [May 13, 2016].
- Golding, M.L., Orchard, M.J., Zonneveld, J.-P., Henderson, C.M. and Dunn, L. (2014): An exceptional record of the sedimentology and biostratigraphy of the Montney and Doig formations in British Columbia; *Bulletin of Canadian Petroleum Geology*, v. 62, no. 3, p. 157–176.
- Lyster, S. (2013): Quantification of uncertainty in shale gas resources; Alberta Energy Regulator. AER/AGS Open File Report 2013-13, 35 p., URL https://www.ags.aer.ca/publications/OFR_2013_13.html [June 2017].
- Moslow, T.F. and Davies, G.R. (1997): Turbidite reservoir facies in the Lower Triassic Montney Formation, west-central Alberta; *Bulletin of Canadian Petroleum Geology*, v. 45, no. 4, p. 507–536.
- Passey, Q. R., Creaney, S., Kulla, J.B., Moretti, F.J. and Stroud, J.D. (1990): A practical model for organic richness from porosity and resistivity logs; *American Association of Petroleum Geologists Bulletin*, December 1990, v. 74, no. 12, p. 1777–1794.

Playter, T.L., Corlett, H.J., Konhauser, K., Robbins, L., Rohais, S., Crombez, V., MacCormack, K.E., Rokosh, C.D., Prenoslo, D., Furlong, C.M., Pawlowicz, J.G., Gingras, M., Lalonde, S., Lyster, S. and Zonneveld, J.-P. (2018): Clinof orm identification and correlation in fine-grained sediments: A case study using the Triassic Montney Formation; *Sedimentology*, v. 65, no. 1, p. 263–302.

Pyrcz, M.J. and Deutsch, C.V. (2014): *Geostatistical reservoir modeling*, 2nd Ed.; Oxford University Press, 433 p.

Zonneveld, J.-P., and Moslow, T.F. (2018): Palaeogeographic setting, lithostratigraphy, and sedimentary framework of the Lower Triassic Montney Formation of western Alberta and northeastern British Columbia; *Bulletin of Canadian Petroleum Geology*, v. 66, no. 1, p. 93–127.